Equilibrium theory of the hard sphere fluid and glasses in the metastable regime up to jamming. II. Structure and application to hopping dynamics

Ryan Jadrich and Kenneth S. Schweizer

Citation: The Journal of Chemical Physics **139**, 054502 (2013); doi: 10.1063/1.4816276
View online: http://dx.doi.org/10.1063/1.4816276
View Table of Contents: http://scitation.aip.org/content/aip/journal/jcp/139/5?ver=pdfcov
Published by the AIP Publishing

Equilibrium theory of the hard sphere fluid and glasses in the metastable regime up to jamming. II. Structure and application to hopping dynamics

Ryan Jadrich[1,2] and Kenneth S. Schweizer[1,2,3,a)]
[1]*Department of Chemistry, University of Illinois, Urbana, Illinois 61801, USA*
[2]*Frederick Seitz Materials Research Laboratory, University of Illinois, Urbana, Illinois 61801, USA*
[3]*Department of Materials Science, University of Illinois, Urbana, Illinois 61801, USA*

(Received 13 April 2013; accepted 7 July 2013; published online 1 August 2013)

Building on the equation-of-state theory of Paper I, we construct a new thermodynamically consistent integral equation theory for the equilibrium pair structure of 3-dimensional monodisperse hard spheres applicable up to the jamming transition. The approach is built on a two Yukawa generalized mean spherical approximation closure for the direct correlation function (DCF) beyond contact that reproduces the exact contact value of the pair correlation function and isothermal compressibility. The detailed construction of the DCF is guided by the desire to capture its distinctive features as jamming is approached. Comparison of the theory with jamming limit simulations reveals good agreement for many, but not all, of the key features of the pair correlation function. The theory is more accurate in Fourier space where predictions for the structure factor and DCF are accurate over a wide range of wavevectors from significantly below the first cage peak to very high wavevectors. New features of the equilibrium pair structure are predicted for packing fractions below jamming but well above crystallization. For example, the oscillatory DCF decays very slowly at large wavevectors for high packing fractions as a consequence of the unusual structure of the radial distribution function at small separations. The structural theory is used as input to the nonlinear Langevin equation theory of activated dynamics, and calculations of the alpha relaxation time based on single particle hopping are compared to recent colloid experiments and simulations at very high volume fractions.
 [http://dx.doi.org/10.1063/1.4816276]

I. INTRODUCTION

In this article, Paper II, we build on the preceding paper[1] (referred to as Paper I) by constructing a thermodynamically self-consistent integral equation theory of the pair structure of hard spheres in 3-dimensions applicable in the metastable regime up to jamming. Our primary interest is the possible equilibrium densest glass that continues the fluid into the metastable regime since it may be relevant to understand *equilibrium* activated hopping dynamics in ultra-dense colloidal suspensions and hard sphere fluids. For structure, we take a different perspective than the replica approach,[2,3] and ask whether relatively simple modifications of equilibrium integral equation theory (IET) can be devised to describe the hard sphere fluid structure in the metastable regime including the limiting jammed state? As input to the IET we use the thermodynamic equation-of-state (EOS) for the 3D densest glass derived in Paper I.[1] We note that very accurate pair structural information is required to fully evaluate the dynamical predictions of the microscopic ideal mode coupling theory (MCT)[4] and the activated barrier hopping nonlinear Langevin equation (NLE) theory.[5,6] These approaches are especially sensitive to the high wavevector behavior of the Fourier-transform of the direct correlation function,[7] and we place special emphasis on this quantity.

From simulations, it is known that the pair correlation function, $g(r)$, acquires multiple distinguishing features[8–13] as the jammed state at packing fraction η_j is approached. (i) The contact value diverges as $g(r=\sigma) \propto (\eta_j - \eta)^{-1}$, where σ is the hard sphere diameter subsequently taken as the unit of length. This feature is connected with the emergence of a delta-function component of $g(r)$ and the formation of $Z_c = 6$ contacts (isostaticity) at jamming in 3-dimensions. (ii) Close to contact, power law behavior holds: $g(r) \propto (r-\sigma)^{-\nu}$ where $\nu \cong 0.5$, although the precise value of the exponent depends on whether rattlers are kept in the analysis.[8–13] A corollary of this behavior and point (i) is the near contact width (w) of $g(r)$ vanishes linearly with the distance to jamming, i.e., $w \propto \eta_j - \eta$. (iii) The second peak of $g(r)$ splits. (iv) A jump discontinuity at $r = 2\sigma$ and a cusp at 3σ is present. (v) "Quasi long range order" emerges corresponding to a large distance power law decay of $h(r) \equiv g(r) - 1 \propto (r/\sigma)^{-4}$, in stark contrast to exponential decay in equilibrium fluids.[9,10]

The above real space structural features have direct implications in Fourier space for the structure factor, $S(k)$, and direct correlation function (DCF), $C(k)$, which are related as $S(k) = 1 + \rho h(k) = (1 - \rho C(k))^{-1}$ where ρ is the number density. "Inverted critical point anomalies"[9,10] exist at small wavevectors corresponding to (vi) the "hyperuniform" behavior $S(k) \propto k$, and (vii) $C(r) \propto -1/r^2$ which implies $-C(k=0) \to \infty$. Note that the DCF has a very long range negative tail at random close packing (RCP) or in the maximal randomly jammed (MRJ) state[9] as seen in Figure 1, which

a)kschweiz@illinois.edu

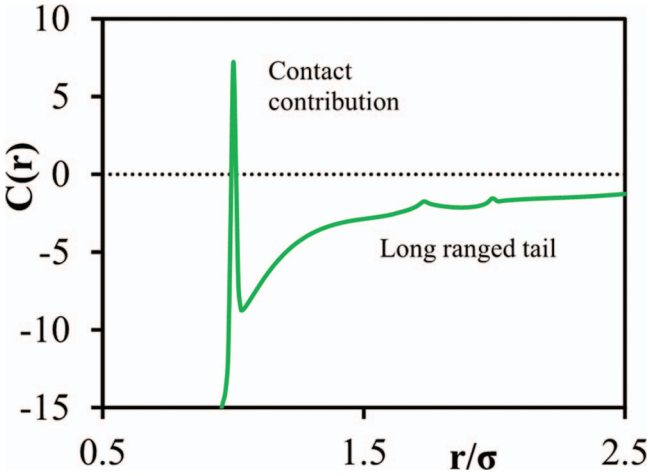

FIG. 1. Direct correlation function of monodisperse jammed hard spheres from simulation.[9] The contact region is divergent, and the long ranged negative tail is not integrable, as jamming is approached.

decays *slower* than the asymptotic behavior of $h(r)$. This feature violates the standard OZ idea that guides closure construction based on the presumed "simpler and shorter range" direct correlation function.[14,15] (viii) As a consequence of the delta-function part of $g(r)$, $C(k)$ decays ultra-slowly for $k\sigma \ggg 1$.

Hopkins, Stillinger, and Torquato[10] have recently shown that remnants of the structural anomalies at jamming discussed above continue to exist significantly *below* the jamming packing fraction under the *nonequilibrium* protocols they employ. They also showed that the unusual features of the pair structure imply a growing static length scale associated with $S(k)$ at small wavevectors, which they speculate plays an important role in glassy dynamics under equilibrium conditions. Of course, the long wavelength structural features are intimately related to the dramatic contact region behavior of $g(r)$ which nucleates a contact force network at jamming.[8] Although the proposal[10] that a growing static length scale in $g(r)$ plays a central role in glassy dynamics is typically dismissed nowadays in favor of a more complex growing amorphous order,[16] it is interesting to recall that criteria for glass formation were formulated years ago[17] based on a local structure analysis.

We demonstrate in this paper that good progress can be made based on IET for the more local structural aspects discussed above: specifically, points (i), (iv), and (viii), and more roughly for points (ii) and (vii). The evolution of these local structural features in an equilibrated fluid (well) below jamming, in contrast to the long wavelength anomalies, are key to capture the full implications of NLE theory for activated dynamics, elasticity, and rheology in the high packing fraction (up to $\eta \sim 0.58 - 0.60$) hard sphere suspensions typically studied experimentally[18,19] and on the computer.[18,20–24] Capturing the negative tail of $C(r)$, as shown in Figure 1, at very high density is also crucial for a density functional theory (DFT) treatment of crystallization[25] and thermodynamic glass formation.[26]

In Sec. II we briefly review IET and the generalized mean spherical approximation (GMSA) theory that provides our starting point. The key ideas for constructing the new structural theory are presented, with the many technical details and derivations collected in four appendices. For economy of expression, we assume the reader is familiar with Paper I,[1] and the same notations for characteristic packing fractions carefully explained there are adopted in this paper. The relevant basics of the well-documented dynamical NLE approach are also briefly recalled in Sec. II D.[5,6] Our combined thermodynamic EOS[1] and GMSA theory is then applied to study real and Fourier space structure in Sec. III over a range of high packing fractions, and comparisons with jamming simulations are made. Multiple qualitatively new structural features not present in classic OZ theories are identified and trends summarized. The new IET is then employed as input to NLE theory to determine in Sec. IV the consequences of a better structural theory on the relaxation and viscoelastic properties predicted by this dynamical approach. The paper concludes with a discussion in Sec. V.

II. THEORY

A. Integral equation theory background

The classic starting point of IET is the OZ equation:[14,15]

$$h(r) = C(r) + \rho \int C(r')h(|\mathbf{r} - \mathbf{r}'|)d\mathbf{r}', \tag{1}$$

where $C(r)$ is the direct correlation function, $h(r) = g(r) - 1$ is the total correlation function, and ρ is the particle number density. Exact thermodynamic relations exist for the dimensionless pressure or compressibility factor ($Z \equiv \beta P/\rho$, where $\beta \equiv (k_B T)^{-1}$) that emphasize different aspects of pair structure. The virial route is controlled entirely by the most local aspect of fluid structure:[14,15]

$$Z(\eta) = 1 + 4\eta g(1, \eta), \tag{2}$$

where $g_1 \equiv g(1, \eta) = g(1)$ is the contact value of the radial distribution function and, for simplicity, the hard core diameter $\sigma = 1$ unless it is needed to clearly explain units. The compressibility route emphasizes the long wavelength ($k = 0$) collective density fluctuations:[14,15]

$$a \equiv \frac{\partial \beta P}{\partial \rho}|_T = \left[1 + \frac{24\eta}{\sigma^3}\int_0^\infty r^2 h(r)dr\right]^{-1}$$

$$= 1 - \frac{24\eta}{\sigma^3}\int_0^\infty r^2 C(r)dr = S^{-1}(k = 0) = (\rho k_B T \kappa_T)^{-1}. \tag{3}$$

Here we refer to thermodynamic consistency as any approximate theory that predicts the same pressure based on these two different routes. Additionally, the dimensionless inverse compressibility can be related to the hard sphere contact value using the exact relation[14,15]

$$a = 1 + 8\eta g(1, \eta) + 4\eta^2 \frac{\partial g(1, \eta)}{\partial \eta}. \tag{4}$$

The well-known difficulty in IET is finding a second closure relation between $C(r)$ and $h(r)$. There is an enormous

literature on this subject, with the Percus-Yevick (PY) closure being the most common approximation for hard spheres.[14,15] It is based on assuming the DCF has the same spatial range of the bare potential, and hence

$$C(r) = 0, \quad r \geq 1 \tag{5}$$

coupled with the exact impenetrability constraint

$$g(r) = 0, \quad r < 1. \tag{6}$$

OZ-PY theory is reasonably successful up to the freezing transition at $\eta_f = 0.494$ but makes the unphysical prediction that jamming occurs at $\eta_j = 1$. Moreover, positivity of $g(r)$ fails in OZ-PY theory at packing fractions well below typical experimental jamming densities, the contact value is too small (increasingly so as η grows), the cage peak in $S(k)$ is too high in dense fluids, and thermodynamics is route inconsistent.[14,15]

Within the stable fluid regime, the DCF outside the hard core is never zero, but is low amplitude, positive, and short ranged.[27,28] Increasing packing fraction enhances its magnitude and range which begins to become significant as freezing is approached[27,28] including the appearance of small negative contributions.[28] Recent nonequilibrium simulations[9] find qualitative deviations as the jammed state is approached, where $C(r)$ acquires a (near) delta-function at contact and a long range negative tail, as illustrated in Figure 1. OZ-PY theory is a complete failure at/near jamming, and our working hypothesis is that the novel physics near the jammed state influences structure and dynamics of dense equilibrated metastable fluids.

B. Two Yukawa GMSA theory

Creating a better hard sphere IET requires a better direct correlation function tail. We adopt the analytically tractable Generalized Mean Spherical Approximation (GMSA) as a starting point where the tail of $C(r)$ is of a Yukawa form:[29]

$$C(r) = K\frac{e^{-z(r-1)}}{r}, \quad r \geq 1, \tag{7}$$

where K and z are adjustable parameters. Waisman[29] analytically solved OZ-GMSA theory in 3-dimensions in terms of coupled nonlinear algebraic equations. It is common to choose K and z to reproduce known thermodynamic properties of hard spheres. Hoye and Stell[30] later found explicit results for K and z as functions of g_1 and a. Using nearly exact results for the contact value and compressibility in the normal fluid regime resulted in improved structure and thermodynamic consistency was obeyed by construction.

However, the one Yukawa GMSA solution for $K(g_1, a, z)$ and $z(g_1, a)$ is not adequate deep in the metastable regime since it can never account for both the very short range contact contribution and the long ranged tail of the DCF (see Figure 1) which are necessary to capture the unusual long and short length scale structural features as jamming is approached. We explore the simplest improvement by adding one more Yukawa contribution:[31]

$$C(r) = K_\delta\frac{e^{-z_\delta(r-1)}}{r} + K_\infty\frac{e^{-z_\infty(r-1)}}{r}, \quad r \geq 1, \tag{8}$$

where K_δ and z_δ are the contact contribution amplitude and range, respectively, and K_∞ and z_∞ the analogous long ranged tail values. Obviously this mathematical form is not exact at jamming, but we argue below it can usefully mimic much of the key physics.

Equation (8) contains four unknowns. Simplification is first achieved by combining K_∞ and z_∞ into one parameter thereby reducing the problem to three unknowns. This reduction is physically motivated by the long range nature of the DCF tail at (near) jamming.[9] The classic Kac (mean field) potential limiting description[14] is adopted by taking $z_\infty \to 0$ and $K_\infty \to 0$ such that the tail is finite integrable. Defining

$$v_i \equiv 24\eta K_i \int_1^\infty r e^{-z_i(r-1)} g(r) dr \tag{9}$$

and letting $z_\infty \to 0$, allows for the exact replacement of $g(r) \to 1$ in Eq. (9), giving

$$v_\infty = 24\eta\frac{K_\infty}{z_\infty^2}. \tag{10}$$

The v_i parameters arise naturally in the two Yukawa GMSA solution and must be nonzero to alter structure.[31] Equation (10) shows the necessary coupling between the two parameters, $K_\infty \propto z_\infty^2$ as $z_\infty \to 0$, effectively reducing them to one nonzero and finite variable v_∞. Enforcing the long ranged tail limit explicitly in Eq. (8) gives

$$C(r) = K_\delta\frac{e^{-z_\delta(r-1)}}{r} + \left[K_\infty\frac{e^{-z_\infty(r-1)}}{r}\right]_{\substack{z_\infty\to 0 \\ K_\infty \to z_\infty^2 v_\infty/(24\eta)}}, \quad r \geq 1. \tag{11}$$

This result, combined with Eqs. (1) and (6), then yields the DCF inside the hard core

$$\begin{aligned} -C(r) = a + \frac{1}{2}\eta a r^3 + v_\delta\frac{1-e^{-z_\delta r}}{z_\delta r} + v_\delta^2\frac{\cosh(z_\delta r)-1}{2rK_\delta z_\delta^2 e^{z_\delta}} \\ + \frac{1}{4}r\left(-\frac{v_\delta^2 e^{-z_\delta}}{K_\delta} - 24\eta g_1^2 + 2v_\delta z_\delta\right) \\ + v_\infty + \frac{1}{2}v_\infty\eta r^3, \quad r < 1. \end{aligned} \tag{12}$$

Equation (12) is derived in Appendix A from the full *non* mean field Kac solution.[31] In Fourier space the long range tail is zero except at $k = 0$ where it determines the compressibility via Eq. (3). The analytic expression for $C(k)$ is derived in Appendix B.

There are now 3 unknown parameters that define the DCF tail, and hence we require three constraints. We insist the exact inverse dimensionless compressibility "a" in Eq. (3) and the contact value, g_1, are recovered. As the final constraint, we consider the first derivative of the radial distribution at contact, $\Delta g_1 \equiv [dg(r, \eta)/dr]_{r=1}$, which is proportional to the effective force between two colliding particles in a potential-of-mean-force sense.[14,15] There are exact results for Δg_1 up to $\eta = 0.53$,[32] and an interpolation for different glass branches is constructed in Sec. II C. The lengthy analytic solutions for $K_\delta(g_1, a, \Delta g_1)$, $z_\delta(g_1, a, \Delta g_1)$, and $v_\infty(g_1, a, \Delta g_1)$ then can be derived as discussed in Appendix C.

C. Radial distribution function contact derivative

In addition to enforcing the exact behavior of g_1 and a, we need the 3D HS equilibrium fluid contact derivative, Δg_1. Exact Monte Carlo results[32] exist for this quantity up to $\eta = 0.53$:

$$C_f(\eta) \equiv \frac{-\Delta g_1}{g_1} = 9\eta\frac{(1+\eta)}{(2-\eta)}(1 + c_1\eta + c_2\eta^2 + c_3\eta^3), \tag{13}$$

where $c_1 = 0.97991$, $c_2 = -0.81747$, and $c_3 = 6.44203$ and the subscript f denotes fluid. We believe that this analytical expression is a good representation of the *equilibrium* fluid (analogous to assuming the Kolafa[33] or Carnahan-Starling EOS[34,35] are good representations of the fluid phase) up to η_g (glass transition packing fraction) where by definition the fluid EOS based on virial series re-summations is believed to break down and jamming is predicted at an unphysically high η_j.[33–36] As discussed in Paper I,[1] the fluid phase is viewed as composed of many *hypothetical* glassy states of a given complexity, and the transition to a glassy branch allows prediction of the termination of the metastable branch at the jamming packing fraction, $\eta_j \sim 0.64$.

For packing fractions greater than η_g (along a glass branch), Eq. (13) is not useful and an interpolative scheme must be devised. We believe it is best to interpolate not $C(\eta) \equiv -\Delta g_1/g_1$, which must diverge at jamming under equilibrium conditions, but rather the quantity

$$K(\eta) \equiv C(\eta)/g_1 = -\Delta g_1/g_1^2, \tag{14}$$

which remains finite at jamming assuming equilibrium. This is easily realized through the *exact* scaled particle theory (SPT) relation[37]

$$\Delta g_1 = \left.\frac{\partial G(r)}{\partial r}\right|_{r=1} - 24\eta g_1^2(1-\alpha(\eta)), \tag{15}$$

where $\rho G(r)$ is the density of particles a distance r from a tagged particle conditional upon there being no other particle centers at a distance less than r,[37] and $\alpha(\eta) = \langle g(\mathbf{R_1}, \mathbf{R_2}|\mathbf{R_3})\rangle_{S_2}/g_1$ where $\rho g(\mathbf{R_1}, \mathbf{R_2}|\mathbf{R_3})$ is the density of hard spheres at $\mathbf{R_3}$ given that there are hard spheres at $\mathbf{R_1}$, and $\mathbf{R_2}$ in contact.[37] The coordinates $\mathbf{R_1}$,$\mathbf{R_2}$, and $\mathbf{R_3}$ place particles 1 and 2 in contact and particle 3 only in rolling contact with particle 2. The pointed brackets $\langle\cdots\rangle_{S_2}$ denote an average of $\mathbf{R_3}$ over the available surface area of sphere 2 not blocked by sphere 1. The central goal of any SPT is the approximate calculation of $G(r)$. At jamming one has the exact result

$$\alpha(\eta_j) = (Z_c - 1)/Z_c, \tag{16}$$

where Z_c is the contact coordination number, since, on average, Z_c particles are in contact with a central sphere. Eq. (16) arises since $\langle g(\mathbf{R_1}, \mathbf{R_2}|\mathbf{R_3})\rangle_{S_2}$ accounts for extra spheres around particle 2 in addition to the one defined to be in contact. From slow compression simulation studies it is known the contact coordination number tends towards the isostatic value of $Z_c = Z_{c,iso} \equiv 6$ which is the minimum number of contacts to satisfy mechanical stability through force balancing.[8] We are interested in slowly compressed quasi-equilibrium states so we set $Z_c = Z_{c,iso} \equiv 6$ and $\alpha(\eta_j) = 5/6$.

Infinitesimally close to jamming, the contact derivative takes on the simple form

$$\Delta g_1 = -\frac{24\eta_j}{Z} g_1^2, \tag{17}$$

which follows directly from Eqs. (15) and (16) by realizing that $\partial G(r)/\partial r|_{r=1}$ diverges more slowly than g_1^2. The latter argument is not rigorous, but it is widely believed that $G(r)$ is a monotonically increasing function[37,38] and therefore must diverge more slowly than g_1^2 in order for Δg_1 to be negative. In Appendix D we present a new derivation of the equilibrium jamming contact derivative, Eq. (17), for hard spheres using equilibrium statistical mechanics and force balancing at jamming. There we also explicitly verify the validity of Eq. (17) based on using the 3D GMSA solution and the densest glass branch EOS and corresponding η_j.

To proceed, we construct a simple second order polynomial interpolation for the glassy $K_g(\eta)$ at packing fractions between η_g and η_j by first requiring continuity

$$K_g(\eta_g) = K_f(\eta_g) \tag{18}$$

and smoothness

$$\left.\frac{dK_g(\eta)}{d\eta}\right|_{\eta_g} = \left.\frac{dK_f(\eta)}{d\eta}\right|_{\eta_g} \tag{19}$$

across η_g, and that the equilibrium jamming point form of Eq. (17) is recovered

$$K_g(\eta_j) = \frac{24\eta_j}{Z_c}. \tag{20}$$

In principle, any interpolation functional form may suffice. We choose to use a polynomial for $K_g(\eta)$ since $K_f(\eta)$ is well fit by a low order polynomial and we assume simple smooth and continuous behavior between the glass transition and jamming. Pade approximates are unnecessary as there are no di-

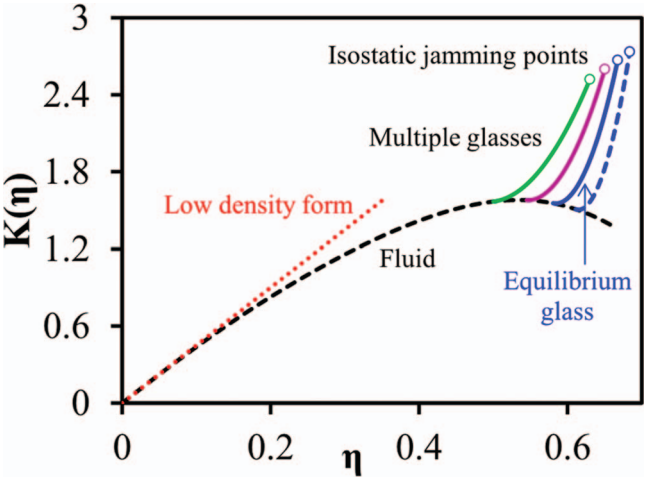

FIG. 2. The non-divergent quantity $K(\eta) \equiv -\Delta g_1/g_1^2$ for the fluid and glassy branches. Dashed red line is the accurate low density form $K(\eta) = 4.5\eta$, thick dashed black curve is the Monte Carlo simulation data of Heyes *et al.*[32] for the fluid. The three solid and thin dashed solid curves are the polynomial interpolating glassy branches, derived according to Sec. II C. The equilibrium jamming point theory predictions of Sec. II C and Appendix D are also shown terminating the glassy branches and we assume isostaticity for the jamming points.

vergences and low order polynomial interpolations have small uncertainties.

Numerical calculations based on Eq. (13) for the equilibrium fluid contact derivative are shown in Figure 2. The polynomial form adopted is given by $K_g(\eta) \equiv w_1 + w_2\eta + w_3\eta^2$ and is combined with the constraints Eqs. (18)–(20); the results in Figure 2 are for four glasses with $\eta_g = 0.5$, 0.545, 0.581, and 0.611 which serve as the fluid continuations to jamming. The fit parameters for the four glasses with increasing glass packing fraction are (i) $w_1 = 13.933$, $w_2 = -50.154$, $w_3 = 50.850$, (ii) $w_1 = 29.812$, $w_2 = -103.358$, $w_3 = 94.600$, (iii) $w_1 = 56.170$, $w_2 = -186.992$, $w_3 = 160.052$, and (iv) $w_1 = 99.177$, $w_2 = -317.715$, $w_3 = 258.371$. We also present in Figure 2 the equilibrium jamming point predictions of Eq. (20) that terminate the glassy branches. We assume the jamming points are isostatic, which is believed to be rigorous for the densest glass branch in 3D.[2,8] The final form for the contact derivative in the fluid and glassy regimes is thus

$$\Delta g_1 = \begin{cases} -g_1^2 K_f(\eta), & \eta < \eta_g \\ -g_1^2 K_g(\eta), & \eta_g \le \eta, \end{cases} \tag{21}$$

where for the rest of the paper $g_1 \equiv g(1, \eta)$ is determined from the equilibrium glass EOS used in Paper I.[1]

We note that based on our thermodynamic theory of Paper I the densest/equilibrium glass corresponding to $\eta_g = 0.581$ and jamming transition at $\eta_j = 0.668$ does not correspond to the zero complexity state at η_K (Kauzmann transition) and η_{GCP} (Glass Close Packing), respectively. We choose to work with the former values in this paper for two reasons: (i) we believe our theory over predicts the location of η_K and η_{GCP} in 3D and (ii) the above values of η_g and η_j agree well with the hybrid simulation-theory results discussed in Sec. III B and Figure 1 of Paper I.[1] However, we have verified that our specific choice of glass branch has little practical impact on our subsequent results since we find glass pair structure is not very sensitive to varying η_g and η_j over a reasonable range, as further discussed in Sec. III A.

Having said the above, we emphasize that our GMSA approach can treat a continuum of glass branches,[1] i.e., for a specific value of η_g there is a unique glass EOS with a unique jamming density η_j. To examine a specific glass branch requires the contact value, g_1, compressibility, a, and contact derivative, Δg_1, as above. These three parameters uniquely determine the three unknown Kac tail GMSA quantities $K_\delta(g_1, a, \Delta g_1)$, $z_\delta(g_1, a, \Delta g_1)$, and $v_\infty(g_1, a, \Delta g_1)$, as discussed in detail in Appendix C.

D. Nonlinear Langevin equation theory

The nonlinear Langevin equation (NLE) theory of single particle activated dynamics has been extensively developed and widely applied over the last decade to analyze the alpha relaxation rate, time correlation functions, elasticity and mechanical response under applied stress of diverse glass and gel forming systems.[5–7] The reader is referred to the literature for detailed discussions. Briefly, the approach is based on a stochastic overdamped equation-of-motion for the scalar displacement of a tagged particle from its initial position, $r(t)$, given by

$$0 = -\zeta_S \frac{dr(t)}{dt} - \frac{\partial F_{dyn}(r(t))}{\partial r(t)} + \delta f(t), \tag{22}$$

where ζ_S is the short time friction constant and the random thermal noise term satisfies $\langle \delta f(0)\delta f(t)\rangle = 2k_BT\zeta_S\delta(t)$. The central quantity is the dynamic free energy, $F_{dyn}(r)$, which quantifies the effective force on the tagged particle from all surrounding particles and is given for spheres by

$$\beta F_{dyn}(r) = -3\ln(r) + \int \frac{d\mathbf{k}}{(2\pi)^3} \frac{\rho C^2(k) S(k)}{1 + S^{-1}(k)} \times \exp\left\{ \frac{-k^2 r^2}{6} \left(1 + S^{-1}(k)\right) \right\}. \tag{23}$$

The first appearance of a minimum in Eq. (23) at $\eta \equiv \eta_c \approx 0.43$ for hard spheres denotes the emergence of transient particle localization[5–7,39] and hence a crossover from fluid-like motion to activated hopping. Equation (22) can be fully solved by stochastic trajectory simulation.[6] Here, we follow the more analytic route based on Kramers theory to compute the mean first passage time for barrier crossing, τ_{hop},

$$\frac{\tau_{hop}}{\tau_0} = \frac{2\pi G}{\sqrt{K_0 K_B}} \exp(\beta F_B), \tag{24}$$

where $\tau_0 = \sigma^2\zeta_0/(k_BT)$, ζ_0 is the dilute limit particle friction constant, K_0 and K_B are the absolute magnitudes of the curvatures (divided by k_BT/σ^2) at the minimum and barrier of $F_{dyn}(r)$, respectively, and $G \equiv \zeta_S/\zeta_0 \cong g_1$ is the ratio of the short time friction to solvent friction computed based on the Enskog binary collision perspective.[5–7] For hard spheres, the time scale of Eq. (24) has been explicitly shown to be tightly correlated with the cage scale relaxation time, τ_α, as measured from the incoherent dynamic structure factor at the first peak of $S(k)$, $F_s(k = k^*, t = \tau_\alpha) = e^{-1}$;[5–7] hence, for high enough barriers ($F_B > 2\,k_BT$), $\tau_{hop} \approx \tau_\alpha$.

Near and below the dynamic crossover volume fraction the barriers are low or nonexistent, and we employ the full Kramers mean first passage time computed as[40]

$$\frac{\tau_\alpha}{\tau_0} = \frac{2G}{\sigma^2} \int_0^d dx \exp(\beta F_{dyn}(x)) \int_0^x dy \exp(-\beta F_{dyn}(y)), \tag{25}$$

where d is the displacement that defines the relaxation event. To mimic structural or cage relaxation, we choose $d \approx 2\pi/k^* = \sigma$.[41]

A microscopic approximation for the shear modulus (in units of k_BT/σ^3) of kinetically arrested solids based on the mode coupling approximation is[42–44]

$$G' = \frac{k_BT}{60\pi^2} \int_0^\infty dk \left[k^2 \frac{d}{dk} \ln(S(k)) \right]^2 \exp\left(\frac{-k^2 r_L^2}{3S(k)} \right), \tag{26}$$

where r_L is the minimum of $F_{dyn}(r)$ or localization length. In reality, activated hopping restores ergodicity on a long enough time scale, but Eq. (26) is an appropriate measure of material rigidity on a time scale before activated events occur.

Finally, NLE theory has been generalized to treat the consequences of applied macroscopic stress, λ, which is modeled as an external microscopic force on particles.[42,43] The latter follows from integrating the stress over the mean particle cross sectional area,[42] resulting in

$$\frac{\partial}{\partial r} F_{dyn}(r;\lambda) = \frac{\partial}{\partial r} F_{dyn}(r) - \frac{\sigma^2 \lambda}{\eta^{2/3}}, \tag{27}$$

where λ is in units of $k_B T/\sigma^3$. An "absolute" yield stress, λ_y, is defined as the minimum stress required to destroy the barrier in $F_{dyn}(r;\lambda)$, which is easily determined from the quiescent $F_{dyn}(r)$ via the maximum restoring force, $f_{max} = \frac{\sigma^2 \lambda_y}{\eta^{2/3}}$.

III. STRUCTURAL PREDICTIONS

A. Radial distribution and direct correlation functions

Perhaps the most stringent test of the present approach is to predict the unusual features of $g(r)$ very close to the jammed state. A possible caveat on such a comparison is our theory is constructed for the metastable equilibrium regime, and all structural features will describe the densest "equilibrium" glass branch corresponding to $\eta_g = 0.581$ and $\eta_j = 0.668$, as discussed in Paper I.[1] However, we do find that structural properties vary little from one glass branch to another, which is consistent with recent simulations that suggest the structure for a range of jamming densities without crystalline order is largely independent of the jamming density or protocol.[45] This non-trivial observation strongly suggests non-equilibrium jammed states probed in simulations are structurally representative of the hypothetical maximally dense equilibrated jammed amorphous state.[45] Hence, our belief (working hypothesis) is that most of the key unusual features of the pair correlation function of a jammed packing are also present in the hypothetical equilibrated fluid/glass close to jamming. This view is supported by the simulations[45] discussed in Paper I[1] which attempt to approach jamming in an equilibrium manner along a densest glass branch that serves as the practical fluid continuation in the metastable regime.

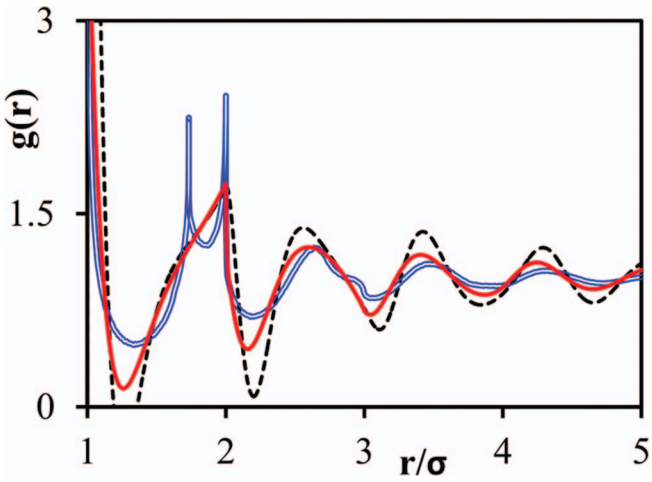

FIG. 3. Radial distribution functions near a jammed state. The open blue curve with a split second peak is the non-equilibrium simulation data of jammed hard spheres.[12,23] The solid red curve is the equilibrium GMSA prediction at $\eta = 0.665$, and the PY result at $\eta = 0.66$ is the dashed black curve.

Figure 3 presents the first comparison, and one sees that the step discontinuity at $r = 2\sigma$ and the cusp-like feature at $r = 3\sigma$ are well captured, a non-trivial consequence of very strong local order. Another success is the ability to accurately predict the damping and shape of the large distance oscillations in Figure 3, in contrast to PY theory which vastly over predicts the strength of these correlations. At small separations, $g(r)$ rapidly decays with increasing r, and the range and shape of subsequent coordination shells are quite well captured. However, one also sees the split second peak is not predicted. We note that the HNC-based replica approach also does not capture this peak splitting.[2] It remains unclear what is missing in the GMSA theory that encodes the peak splitting phenomenon.

What is the functional form of the GMSA pair correlation function close to contact and how does it compare to exact results? Simulations[8–13] of jammed hard spheres find $g(r)$ has two components: (1) a delta function part, $g_\delta(r)$, that rigorously diverges at jamming and accounts for the isostatic six contact neighbors, and (2) a continuously varying contribution slightly beyond contact termed the near contact background contribution, $g_{nc}(r)$, which accounts for the roughly six additional first coordination shell neighbors. Right at jamming, $g_\delta(r) = Z_c \delta(r-1)/(4\pi\rho)$ and $g_{nc}(r)$ is a simple inverse power law:[8–13]

$$g_{nc}^{-1}(r) = A(r-1)^\theta. \tag{28}$$

Combining this with $g_\delta(r)$ for the radial distribution function near contact yields

$$g(r) = \frac{Z}{4\pi\rho}\delta(r-1) + \frac{1}{A(r-1)^\theta}, \quad r \approx 1, \tag{29}$$

where $\theta \approx 0.5 - 0.6$. For jammed spheres, at $\eta_j \approx 0.625$ (after removing rattlers) Torquato *et al.*[12] found the functional form

$$g_\delta(r) = g_1 \left(\frac{6A}{((r-1)/\chi + C)^4} + \frac{B}{((r-1)/\chi + C)^2} \right), \tag{30}$$

where $A \cong 3.43$, $B \cong 1.45$, $C \cong 2.25$ are constants and $\chi \equiv 1 - (\eta/\eta_j)^{1/3}$. The exact mathematical forms of Eqs. (28)–(30) are not captured by the equilibrium and analytic GMSA theory as seen from Figure 4. GMSA predicts that both $g_\delta(r)$ and $g_{nc}(r)$ decay exponentially near contact

$$g(r) = a_\delta e^{-b_\delta(r-1)} + a_{nc} e^{-b_{nc}(r-1)}, \quad r \approx 1, \tag{31}$$

where $a_\delta \gg a_{nc} > 0$ and $b_\delta \gg b_{nc} > 0$, with the first exponential associated with the delta-function-like contribution. As shown in Figure 4, the delta function contribution becomes sharper as jamming is approached and the exponential behavior is evident. Near jamming, $a_\delta \to g_1$ and $b_\delta \to \frac{24\eta}{Z_c} g_1$, and thus from Eq. (31)

$$g_\delta(r) = g_1 \exp\left(-\frac{24\eta}{Z_c} g_1 (r-1) \right), \tag{32}$$

which decays more rapidly than Eq. (30). It is interesting to note that simulations of jammed FCC crystals find $g_\delta(r)$ decreases in a Gaussian manner.[12] Hence Eq. (32) decays at a rate intermediate between jammed amorphous (Eq. (30)) and crystalline states studied via simulation.

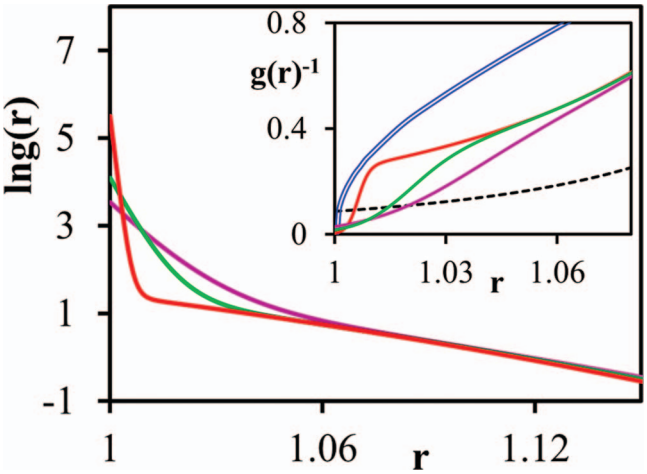

FIG. 4. Natural log-linear plot of the GMSA theory radial distribution function contact region where solid red, green, and purple (decreasing values near contact) curves represent $\eta = 0.665$, $\eta = 0.655$, and $\eta = 0.645$, respectively. Inset: Expanded view of the near contact region plotted as the inverse pair correlation function. Same solid red, green, and purple (decreasing step near contact) curves as in the main frame. Additional open blue and dashed black curves are jammed simulation data[12,23] and PY results at $\eta = 0.66$, respectively.

From Eq. (31) the analogous GMSA prediction for the $g_{nc}(r)$ term is

$$g_{nc}^{-1}(r) = \frac{1}{a_{nc}} \exp\left(b_{nc}(r-1)\right) \tag{33}$$

and unlike Eq. (28) does not diverge at contact. The relatively large differences between the simulation and equilibrium GMSA results close to contact are shown in the inset of Figure 4. In the theory there are two distinct regimes: (i) the hole-like feature very close to contact due to the *finite* width delta-function-like contribution (we are not exactly at jamming), and (ii) the near contact background contribution which grows more strongly than as Eq. (28). The reason for these discrepancies is the exponential functional form in Eqs. (31)–(33). To further test our theory it would be interesting to compare the local structural differences between GMSA theory and an *equilibrated fluid* near, but below, jamming. Such a comparison may be possible using replica exchange Monte Carlo as done for binary hard sphere mixtures.[20]

We further study the predictions of GMSA theory in the delta-function region by computing an integrated measure of local structure, the spatially resolved coordination number:

$$Z_c(r) = 4\pi\rho \int_1^r R^2 g(R) dR. \tag{34}$$

In simulations,[8–13] at contact there is a step function change from zero to $Z_c(r=1) = Z_{c,\,iso} \equiv 6$ because of the delta function in Eq. (29), and then a much slower growth with increasing separation associated with $g_{nc}(r)$. Figure 5 shows the simulation verified functional form:[8–13]

$$Z_c(r) = \begin{cases} 0, & r < 1 \\ Z_{c,iso} + 11\,(r-1)^{0.6}, & r \geq 1, \end{cases} \tag{35}$$

along with the behavior predicted by the PY and GMSA theories. For the latter, results are shown at three packing fractions along the densest glass branch: $\eta = 0.645$, 0.655, and 0.665. One sees that $Z_c(r)$ tends to a step function at contact indicating integrable delta-function-like behavior. Despite the differences between Eqs. (28)–(30) and Eqs. (31)–(33), the corresponding $Z_c(r)$ functions are fairly similar. As expected, integrated features of the jammed state pair correlation function are less sensitive to the theoretical approximations. The functional form (at jamming) for $Z_c(r)$ predicted within the GMSA approach near contact corresponds to

$$Z_c(r) \cong \begin{cases} 0, & r < 1 \\ Z_{c,iso} + \dfrac{a_{nc}\left(2 + 2b_{nc} + b_{nc}^2 + e^{b_{nc}(r-1)}\left(-2 - r b_{nc}\left(2 + r b_{nc}\right)\right)\right)}{b_{nc}^3}, & r \geq 1. \end{cases} \tag{36}$$

Overall, the GMSA theory is enormously better than PY theory near jamming, and many results agree qualitatively with jammed hard sphere simulations. The main differences are the much faster decaying delta function and near contact background term in the pair correlations.

It is well known that the contact region of $g(r)$ is strongly correlated with the mechanical properties of a hard sphere packing.[12,45,46] For example, the interparticle force, f, probability distribution, $P(f)$, is related to $g(r)$ via a Laplace transform.[12,45,46] Large forces correspond to very small interparticle separations, and weak forces the converse. From Figure 5 it is clear that the power law form of Eq. (35) is *not* well captured by the GMSA approach. Specifically, the amplitude of the longer ranged tail of $Z_c(r)$ is too large, which results in too large of a weak force regime. Interestingly, the small cage replica method is also not able to fully capture the weak force regime, incurring errors in the same qualitative direction as GMSA theory.[2,45] On the other hand, large forces are controlled by the delta-function regime, $g_\delta(r)$, which is shown in the inset of Figure 5. The simulation observed functional form, Eq. (30), with the above A, B, and C parameters, is also shown and compared to GMSA and small cage replica theory[2,45] calculations based on using our densest/equilibrium glass EOS as input. Interestingly, we find all 3 results are very similar. There is a small upturn in the GMSA result at larger separations, but this feature would move further outwards if we could numerically get closer to the jamming transition. Overall, we conclude that GMSA theory does

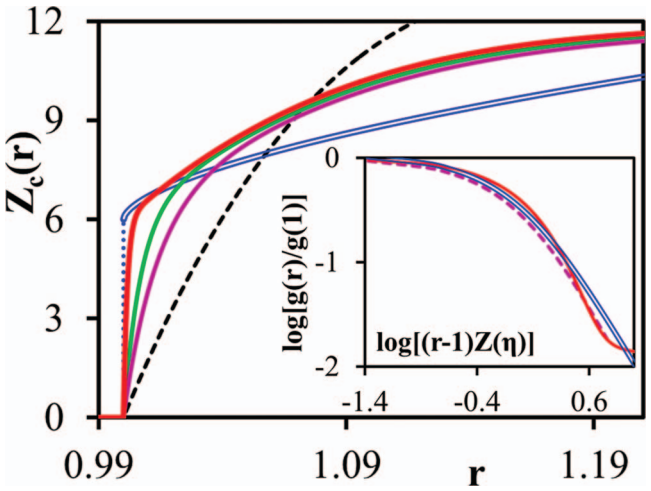

FIG. 5. Coordination number as a function of inter-particle separation where solid red, green, and purple (decreasing step near contact) curves represent GMSA results at $\eta = 0.665$, $\eta = 0.655$, and $\eta = 0.645$, respectively. Open blue and dashed black curves are jammed simulation data[12,23] and PY results at $\eta = 0.66$, respectively. Inset: Zoomed in view of the delta function region of the radial distribution function, $g_\delta(r)$, where solid red, open blue, and dashed purple are GMSA, simulation,[12] and replica theory (RT) results,[2,45] respectively; all three are at $\eta = 0.665$ (close to jamming) using our densest glass equation of state for g_1.[1] For the simulation result, we have assumed that the three parameters A, B, and C in Eq. (30) are effectively constants and use the values determined via simulation in Ref. 12.

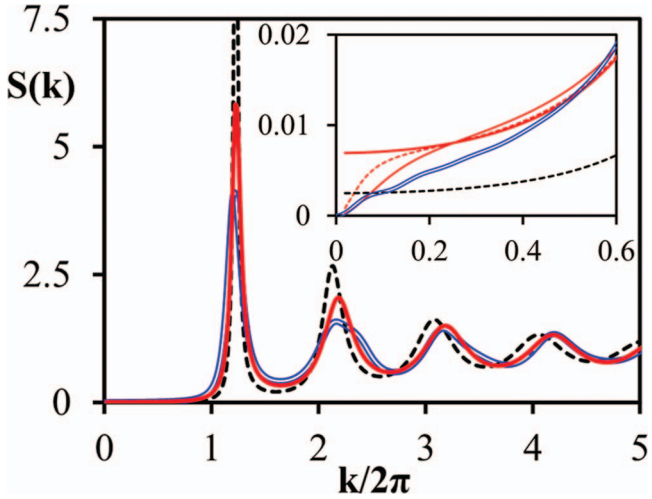

FIG. 7. Static structure factor comparison between theory and simulation. Solid red, open blue, and dashed black curves are the GMSA theory ($\eta = 0.665$), jammed simulation,[9,12,23] and the PY theory ($\eta = 0.66$), respectively. The red and open blue curves overlap well hiding most of the open blue curve. The off scale value of the PY primary structure factor peak is 8.7. The inset shows an expanded view of the low wave vector region where the color and line conventions are the same as in the main frame. Two additional curves, thin red solid and dashed, correspond to including first order mean field finite tail corrections using $z_\infty = 0.01$ and $z_\infty = 0.02$, respectively.

a good job of capturing the large interparticle forces, as does the replica approach, but neither theory accurately captures the weaker forces.

Figure 6 compares the PY and GMSA approaches in the stable and metastable regions. Clear differences at $\eta = 0.6$ are apparent, but for $\eta = 0.5$ we find a nearly perfect agreement which gets better as the packing fraction is further lowered. This latter trend is not surprising since at lower η the compressibility (contact value) is larger (smaller) leading to small values of K_δ and v_∞ whence the PY direct correlation approximation becomes rather accurate. Beyond $\eta \approx 0.6$, the

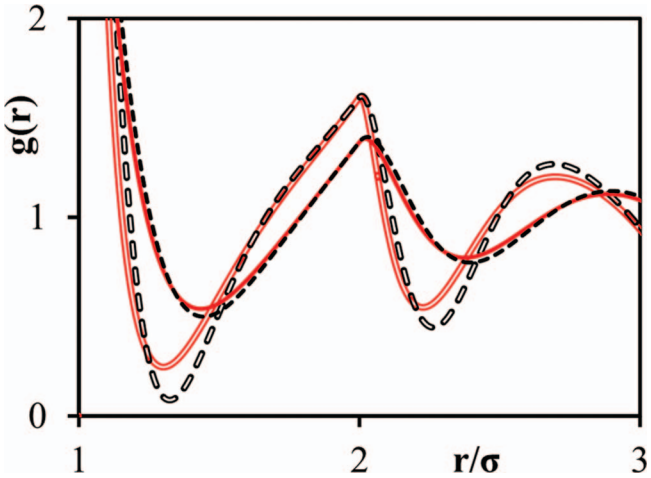

FIG. 6. GMSA pair correlation function compared to its PY analog at high and intermediate volume fractions. The solid red and solid dashed black curves that overlap almost perfectly are the GMSA and PY results at $\eta = 0.5$, respectively. Open curves are analogous results for $\eta = 0.6$, showing a clear difference between PY and GMSA predictions.

OZ-PY results become unphysical since $g(r) < 0$ for some separations.

Finally, one can ask whether the GMSA theory predicts a negative tail in $C(r)$ as seen in the simulations of Figure 1. Comparing the infinitesimal amplitude, but infinitely long range, GMSA mean field tail to that in Figure 1 may seem confusing, but its sign follows from v_∞ or Eq. (10) which is controlled solely by K_∞. GMSA theory predicts a negative tail which grows in amplitude (v_∞ grows) as packing fraction is increased. To our knowledge, no simulation data are currently available that precisely establishes when this tail becomes negative. However, existing results do show negative regions of the fluid direct correlation function emerge in the equilibrium state around the freezing packing fraction.[28] While the extremely long ranged negative tail has only been seen in simulations of jammed states,[9,10] prior DFTs of a thermodynamic glass transition[26] and equilibrium melting[25] required the ad hoc postulate of negative DCF tails to be successful. This prior work seems consistent with our structural theory which addresses the metastable amorphous regime.

B. Structure factor and Fourier-space direct correlation function

Overall, reasonable agreement is found between the simulation and GMSA theory results for $g(r)$, though there are discrepancies. However, in k space, Figure 7 shows that the difference between theory and simulation arising from the second peak region and near contact background term in $g(r)$ is averaged over by the Fourier transform and better agreement with simulation is found for $S(k)$. There is good agreement between the location, shape and breadth of the primary cage peak, though the magnitude is larger than in simulation. The over predicted peak magnitude may be due to the full

equilibration of structure in the theory which favors stronger local ordering. Such behavior has been seen in simulations of dense polydisperse hard spheres where initially the first diffraction peak is relatively small due to non-equilibrium effects, and grows in magnitude upon equilibration.[24] However, we again note that recent simulations suggest the equilibrium nature of our theory cannot account for the structural discrepancies near jamming[45] implying key physics is still missing in our theory. On the other hand, the calculations based on PY theory in Figure 7 are very poor for this first peak, greatly over-predicting its magnitude, an error in the opposite direction made for $g(r)$ at contact. Note that PY theory becomes even worse at higher k, where subsequent peaks occur at increasingly wrong locations with amplitudes that are far too low. Strong high k correlations are a signature of the jammed state, and the GMSA calculations agree very well with simulation in terms of peak locations and damping of the amplitudes. This is a direct consequence of the more accurate near contact region in $g(r)$.

The intermediate wave vector predictions of GMSA theory for $S(k)$ are also in very good agreement with simulation except at the second peak. Simulation finds a small asymmetry or shoulder in the second peak, which is absent in theory. This feature may also be related to the absence of a split second peak in $g(r)$ of the GMSA theory. But, as expected (and indeed is inevitable), qualitative deviations between GMSA theory and simulation for $S(k)$ are present at *very low* k as seen in the inset of Figure 7. Nonequilibrium simulations find a non-liquid-like quasi-linear growth as $k \to 0$, the consequences/implications of which have been thoroughly discussed in the literature.[9,10] GMSA theory cannot capture this behavior since it is an analytic equilibrium approach which leads to the expected quadratic growth of the structure factor at small wavevectors; moreover, the r^{-2} power law of the long range DCF tail is not captured.

One subtlety should be noted pertaining to the magnitude of the low k GMSA results in the inset of Figure 7. It would seem from the plot that the GMSA $S(k = 0)$ is *larger* than the PY analog, but this is simply the consequence of the infinitely long range tail (Kac) approximation adopted which implies only a contribution at exactly $k = 0$ is present (see Appendix B). While the overall magnitude of the GMSA $S(k)$ in the inset of Fig. 7 is larger than the PY analog at low wavevectors, the exact $k = 0$ value is much smaller and must be analytically added in by hand. To achieve this, a first order correction to the mean field tail has been included by assuming $z_\infty = 0.01$ and 0.02 in the inset of Figure 7. Even with this correction, agreement with simulation is not perfect, but the overall shape of the GMSA and simulation $S(k)$ curves are quite similar and the differences may stem from the equilibrium nature of the theory.

Below jamming there are no delta-function contributions to the pair correlation function, and $C(k)$ has a simple and exact high k limiting form for hard spheres:[47]

$$C\,(k \to \infty) = 4\pi g_1 \frac{\cos(k)}{k^2}. \tag{37}$$

It is of interest to determine how high k must be reached before this relation holds, especially since this function plays a central role in the dynamical vertex of NLE theory[5–7] (see Eq. (23)). This motivates re-plotting the calculations in Figure 7 as $k^2|C(k)|$, as shown in Figure 8, a representation that amplifies differences between various theories, and also simulation, especially on very small length scales.

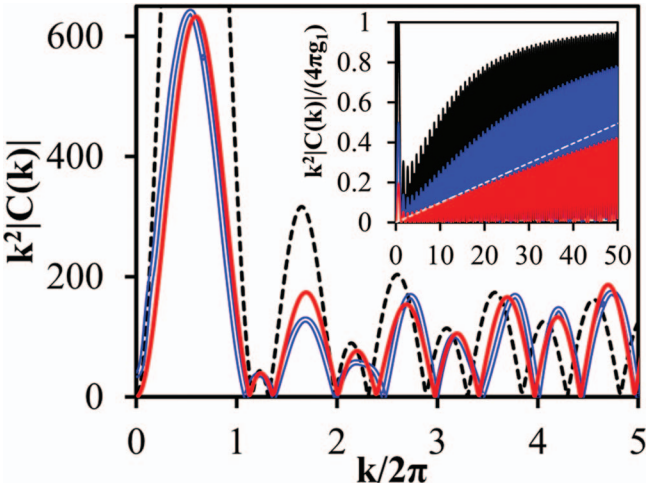

FIG. 8. Absolute value of the k-space direct correlation function multiplied by dimensionless wave vector squared. The solid red, open blue, and dashed black curves are results for the GMSA theory ($\eta = 0.665$), jammed simulation,[9,12,23] and PY theory ($\eta = 0.66$), respectively. The simulation system is almost perfectly jammed, but upon removing "rattler" particles the final $\eta \sim 0.6275$; this value was employed to convert from $S(k)$ to $C(k)$. Varying the assumed simulation value of η from 0.62 to 0.644 does not result in any significant change of our results nor our dynamical theory conclusions in Sec. IV. Inset: Same as main frame, but the ordinate is divided by the asymptotic large wavevector limit value. GMSA theory results are shown at (bottom to top) $\eta = 0.665$ (red), $\eta = 0.66$ (blue), and $\eta = 0.65$ (black). The dashed white line highlights the increasing long linear regime found as jamming is approached.

Figure 8 shows that the GMSA theory is accurate in the lower k regime, whereas PY theory fails completely and strongly over predicts the first peak. The only (weak) difference between the GMSA prediction and simulation is the location of the first low k peak. Beyond this first peak region, which is associated with the first oscillation of the DCF at a wavevector well below the cage peak of $S(k)$, the GMSA and simulation results agree quite well in terms of peak location and magnitudes. On the other hand, the PY theory results for the location of the oscillations and their magnitudes are poor. There is strong damping with increasing wavevector for PY, whereas both the GMSA and simulation results show an interestingly different behavior. Specifically, an almost linear increase with wavevector of the second, fourth, and subsequent even numbered maxima is found. This linear behavior starts at the origin ($k = 0$) and extends up to increasingly high wavevectors as the volume fraction grows in the metastable regime. As discussed in the next section, Sec. IV, such behavior has large implications for dynamical theories that emphasize local physics such as NLE theory.[5–7]

To examine in more detail how high in wavevector the above linear behavior extends within GMSA theory, we plot in the inset of Figure 8 the quantity

$$\frac{k^2\,|C(k)|}{4\pi g_1} \overset{k\to\infty}{\to} |\cos(k)|, \tag{38}$$

for $\eta = 0.65$, 0.66, and 0.665. This format makes it easier to see the linearity of $k^2|C(k)|$, as well as when the asymptotic limit of Eq. (37) is approached. Linear behavior is found up to $k/(2\pi) \approx 5$, 10, and 25 for $\eta = 0.65$, 0.66, and 0.665, respectively. Approaching jamming greatly extends the range over which $C(k) \propto k^{-1}$, and the range appears to diverge in the jamming limit; for example, from the inset of Figure 8 one sees that at $k/(2\pi) = 50$, Eq. (37) is still not valid even at the lowest volume fraction studied. Effectively the known asymptotic limit $C(k) \propto k^{-2}$ may be replaced with $C(k) \propto k^{-1}$ at or near (for practical purposes) jamming. Unfortunately, simulations have not yet probed this very high k regime due to computational difficulties.[8–13]

The $C(k) \propto k^{-1}$ behavior is directly related to the vanishing length scale in $g_\delta(r)$ as jamming is approached. This follows from the fact that in the high wavevector regime of interest, $h(k) \to C(k)$, and if $g(r)$ is a delta function at contact then $h(k) \propto k^{-1}$ in 3-dimensions. Of course, below jamming there is no delta-function, however if the width, w, of the sharp feature of $g(r)$ is small compared to the wavevector it will effectively appear as a delta function and thus one expects $C(k) \propto k^{-1}$ for $kw < 1$. It would be interesting to test our results for the $C(k) \propto k^{-1}$ behavior against future simulations.

IV. NLE-GMSA THEORY DYNAMICAL PREDICTIONS

A. Alpha relaxation time

Recent dynamical simulations of Berthier and Tarjus have aimed to incisively test NLE theory for repulsive force and hard sphere fluids based on using simulation structural input.[48] The theory was found to strongly underpredict the growth of the relaxation time at low temperatures or very high packing fractions. There are two caveats on this conclusion: (i) the simulations studied mixtures while the theory utilized is for one-component systems, and (ii) the theory requires structural information (direct correlation function) to increasingly high wavevectors as volume fraction grows, information that may not be possible to accurately determine in simulation. Point (ii) was the major motivation for the development of the new structural theory in this paper. To further explore these issues, we employ the GMSA structural input in NLE theory, and contrast its predictions with prior work that employed PY theory,[5,6] and recent experiments on hard sphere colloid suspensions performed to exceptionally high volume fractions and the corresponding simulations.[18] A caveat is the experiments and simulations are for polydisperse systems. However, it is widely accepted that polydispersity reduces the relaxation time[18,41] (at least at very high volume fractions) relative to the monodisperse case, and hence an accurate theory for the latter should presumably overpredict the relaxation time growth with compaction.

Our calculations of the mean alpha relaxation time using NLE-GMSA theory are shown in Figure 9. At low packing fractions where there is no barrier ($\eta \leq 0.43$, normal fluid regime), the theory is very accurate. It also is quite accurate in the extended crossover regime from $\eta \sim 0.45 - 0.57$, corresponding to a growth of the relaxation time by roughly 4 orders of magnitude up to entropic barriers of $\sim 7\, k_B T$. However, at even higher concentrations the theory significantly under predicts the relaxation time, as clearly seen in the inset. This too slow growth of the relaxation time occurs despite the fact the GMSA-based NLE theory predicts a divergent barrier and relaxation time at jamming which is now located at a reasonable packing fraction.[1]

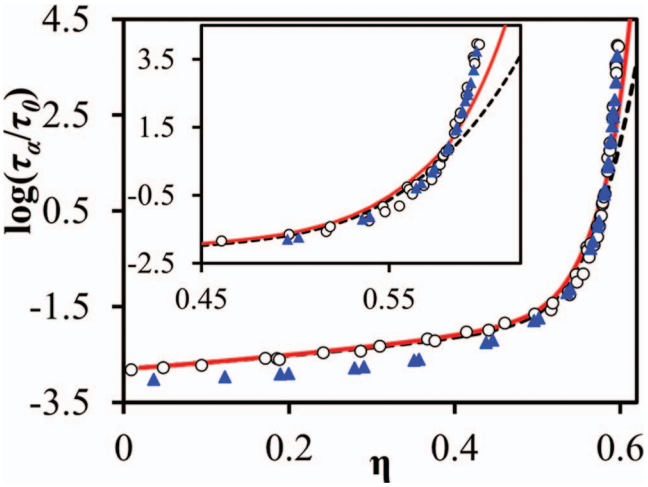

FIG. 9. Dimensionless alpha relaxation time as a function of packing fraction. Solid red (dashed black) curve is the NLE theory result based on GMSA (PY) structural input. The open circles and blue triangles are the experimental and simulation results, respectively.[18] The inset is an expanded view of the high packing fraction regime.

Figure 9 also shows that use of the more accurate GMSA structure makes a major difference compared to the prior PY based dynamical predictions for $\eta \geq 0.55$, improving the results compared to experiment and simulation. This clearly establishes the importance of $C(k)$ at very high wavevectors and serves as a caution in attempts to use simulation structural input. The latter point is further illustrated by implementing NLE-GMSA theory in a way that high wavevector information in the dynamical vertex of Eq. (23) is removed by hand via an upper wavevector cutoff at k_c. Although not plotted here, we find that significant errors are incurred if the cutoff is too small, always in the direction of too small a relaxation time, which worsens as packing fraction grows. Indeed, a *very* large cutoff of $k_c = 80$ (over 10 times beyond the cage peak) is required to capture the full NLE predictions in Figure 9. This crucial importance of high wavevectors is not surprising given the nature of NLE theory which prior analytic ultra-local analysis has shown is based on local cage scale physics.[7]

Regardless of the possible issues of using inaccurate theoretical or simulated structural information at high wavevectors, we do believe that Figure 9 shows that NLE theory, in its current form, is missing some key physics at very high volume fractions associated with longer length scale "collective" effects. To further buttress this conclusion, we present an "Angell plot" in Figure 10 of τ_α versus $Z(\eta)$, as suggested by Berthier and Tarjus.[48] In this format the apparent collapse of all hard sphere dynamical data regardless of polydispersity can be achieved.[41] Figure 10 shows the NLE-GMSA results and simulation data overlap well up to $Z \sim 20$. One again sees that the theory becomes increasingly inaccurate at higher Z in the direction of too weak fragility. The analogous NLE

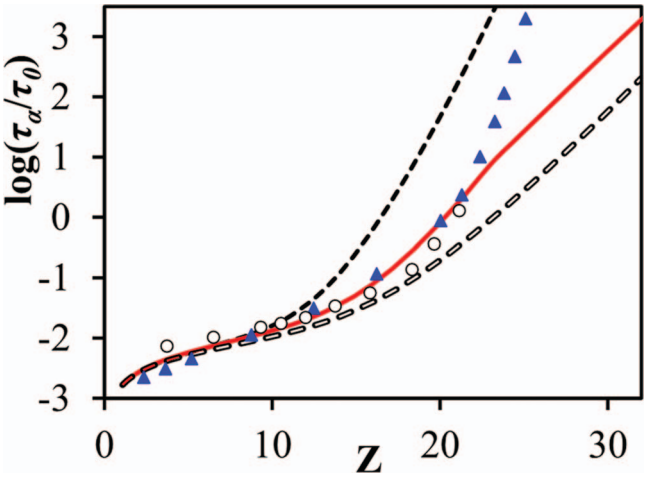

FIG. 10. Angell-like plot of the same results of Figure 9 where Z is the compressibility factor. The solid red curve is the NLE-GMSA result while open circles and blue triangles are the simulations of Sear *et al.* for a polydisperse system[41] and the binary mixture of Berthier and Witten,[21] respectively. The solid and open dashed curves employ PY theory in NLE theory and Z computed using the pressure and compressibility routes, respectively.

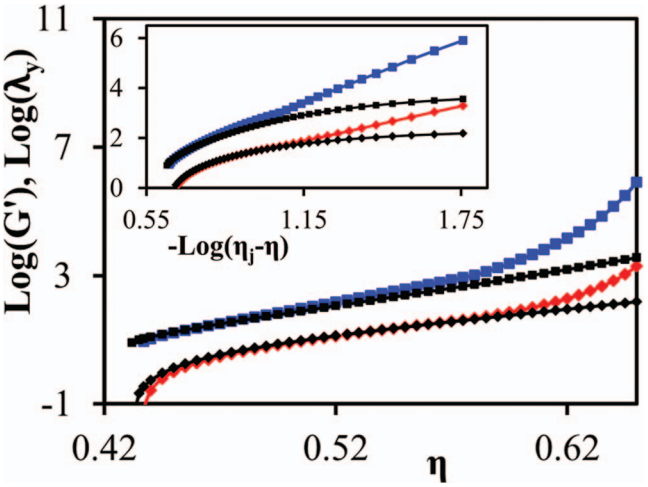

FIG. 11. Dimensionless shear modulus (blue squares) and absolute yield stress (red diamonds) as a function of packing fraction based on GMSA input to the NLE theory. The analogous PY-based results are depicted by smaller black (dark) squares and diamonds, respectively. Connecting curves are guides to the eye. Inset: Same as the main frame except re-plotted in a log-log format with the x-axis the distance of the packing fraction from jamming.

results based on PY structural input, with Z computed via the virial and compressibility routes, is also shown. Although all three of the theoretical curves differ, they share the trend of significantly too slow growth with Z at very high packing fractions. Work is in progress to generalize the microscopic NLE approach to include the missing spatially longer range collective dynamical effects.[49]

Finally, we comment on the role of mean field thermodynamic singularities in activated relaxation theories. Entropy crisis approaches, such as the Adams-Gibbs and random first order transition (RFOT) theories,[16] predict a divergent barrier and relaxation time when the configurational entropy or complexity vanishes. For monodisperse hard spheres this occurs at η_K, which in 3D has been estimated based on replica theory and our approach[1] as $\eta_K \approx 0.61$. Thus, one might worry that our calculation of a relaxation time beyond this Kauzmann density is ill-defined or contradictory. However, we are analyzing dynamics based on the NLE approach, which is not a thermodynamics-based theory, and which has no dynamical divergences below jamming.[5] Based on Paper I, jamming occurs at $\eta_{GCP} \approx 0.68$. Hence, there is no contradiction since we are using our thermodynamic theory[1] solely as technical input to construct the structural GMSA theory, which in turn quantifies the dynamical vertex of NLE theory. More generally, whether barriers diverge at the zero complexity state, generally argued to be below jamming,[2,16] is not a question amenable to definitive resolution for many reasons including the inability to experimentally probe ultra-large relaxation times and the unknown validity of a thermodynamic Kauzmann transition let alone it precise location if it does exist.

Now, if one does adopt the widely quoted expression[50] of the alpha relaxation time of thermal liquids from RFOT, $\tau_\alpha = \tau_0 e^{B/S_c}$ with $B = 32$, assume it applies to hard spheres, and uses our theoretical result for the configurational entropy, then we find (not plotted) that the predicted alpha times are much larger and much too strongly increasing with packing fraction compared to the simulation and experimental data in Figures 9 and 10. Of course, this conclusion is not really definitive since the RFOT relaxation time is very sensitive to both the value of B and the precise packing fraction of the zero complexity state. One could empirically vary one or both of the latter parameters with the goal of fitting data. However, such an exercise is not in the spirit of our present fully *a priori* confrontation of NLE theory with experiment and simulation.

B. Elasticity and yielding

Mechanical property calculations based on both GMSA and PY structural input are shown in Figure 11. One sees that the absolute yield stress, λ_y, and linear shear modulus, G', are *not* sensitive to which IET is employed up to packing fractions of ~0.57. Note these properties probe different, shorter length scale aspects of the dynamic free energy, in the interval from the localization length to well below the barrier location.[5–7] At higher packing fractions, serious deviations between the two NLE predictions are found depending on equilibrium input, with the GMSA-based results always displaying a stronger growth with packing fraction, the same trend found for the mean barrier hopping time.

Very interestingly, the inset of Figure 11 shows that the GMSA based results follow a power law over a wide range of volume fractions that shows no sign of being cutoff as jamming is approached. This behavior, and the apparent growth of G' as $(\eta_j - \eta)^{-4}$, are in good agreement with both recent experiments that measured the elastic modulus of repulsive colloid suspensions[51] and the prior analytic analysis of naive MCT.[7]

V. SUMMARY AND CONCLUDING REMARKS

We have developed a new thermodynamically consistent integral equation theory for the equilibrium pair structure of hard sphere fluids in the metastable regime between the freezing and jamming densities. Essentially exact behavior of the

contact value of the pair correlation function and isothermal compressibility are enforced, along with a new analytic expression for the equilibrium jamming contact derivative. The approach employs the two Yukawa GMSA approximation for the direct correlation function beyond contact, motivated by the desire to at least qualitatively capture the unusual features of the DCF as the jammed state is approached. The existence of a very long range negative tail of the DCF in jammed packings motivated our use of a Kac-like mean field treatment of one of the tails. The other Yukawa tail is very intense and short range and is meant to capture the emergence of a delta-function-like feature at contact in $g(r)$. As input to the structural theory we use our thermodynamic scaled particle theory of Paper I[1] to predict the densest glass branch EOS which serves as the practical metastable continuation of the fluid EOS.

Comparison of the equilibrium theory with the simulation $g(r)$ in the jammed limit reveals reasonably good agreement for many of the local structural features discussed in the Introduction. However, neither a split second peak nor a power law form near contact of the pair correlation function is captured. However, such differences have significantly less practical impact in Fourier space where calculations of the structure factor and DCF, from below the first cage peak up to very high wavevectors, agree very well with simulation as jamming is approached. In Fourier space, the oscillatory DCF decays very slowly at high wavevector in the high volume fraction regime, a consequence of the unusual near contact structure of $g(r)$. Of course, the non-analytic hyperuniform (inverted critical point)[9,10] behavior of $S(k)$ at low wavevectors is not captured within our analytic equilibrium framework.

From a broader perspective, we find it interesting that by enforcing the pressure predicted from the virial and compressibility routes to agree and be exact, along with what we believe is a good approximation for the contact derivative, many nontrivial features of the pair correlation function and structure factor can be recovered. The GMSA theory predicts a negative tail in the direct correlation function, qualitatively consistent with simulations that find in the stable fluid the DCF had a small positive tail,[28] while at jamming a long range negative tail emerges.[9] By implication, we are suggesting the latter exists in the highly compressed (metastable) equilibrium fluid below jamming. Indirect support for this view follows from prior DFT theory studies of crystallization[25] and thermodynamic glass formation[26] of hard spheres.

We emphasize that our primary interest is neither nonequilibrium nor jammed systems, but rather very dense equilibrated hard sphere fluids and colloidal suspensions that display slow activated glassy dynamics. This corresponds to volume fractions far above freezing, but significantly below jamming. In this regime there are many qualitative deviations between the structural predictions of the new GMSA theory and classic IETs. The present approach may also find value in treating the structure of soft repulsive fluids at very high effective densities within a perturbation framework.[52] As discussed in Sec. IV, the differences between GMSA theory and classic IET approaches have strong implications on the predictions of the NLE theory of single particle barrier hopping and elastic properties at high packing fractions which requires highly accurate structural information in Fourier space up to very large wavevectors of order an inverse transient localization length, a quantity which diverges in the jamming limit.[5–7]

Concerning future improvements of the structural theory, perhaps the most tractable avenue for progress that is relevant to the well below jamming regime is to formulate a better interpolation formula for the derivative of the pair correlation function at contact along a glassy branch. This aspect has a large influence on the delta-function-like region near contact in $g(r)$, and improvement will impact the high k region of $C(k)$. It is also desirable to investigate a non-mean field Kac potential form for the slowly decaying tail of $C(r)$. Additionally, the GMSA theory should be generalizable to mixtures, and perhaps higher dimensionality. The latter would be an especially large undertaking since it is unclear whether the rather complex mathematical methods that allow an analytic solution of the OZ equation with the double Yukawa MSA closure in 3D can be extended to higher dimensions. If this can be achieved, then it would allow one to also reliably extend the NLE theory analysis to higher dimensions, an interesting direction for future research.

ACKNOWLEDGMENTS

We acknowledge informative and stimulating discussions and correspondence with Sal Torquato. We also thank Professor Torquato for sending us the numerical jamming simulation data presented in our figures, and for sending us a preprint of Ref. 10. We also thank Richard Sear, Ludovic Berthier, and Luca Cipelletti for sending us their numerical relaxation time data used in Figures 9 and 10. Finally, we thank both reviewers of the paper for their constructive and valuable criticisms and suggestions. This work was supported by DOE-BES under Grant No. DE-FG02-07ER46471 administered through the Frederick Seitz Materials Research Laboratory.

APPENDIX A: DERIVATION OF THE REAL SPACE DIRECT CORRELATION FUNCTION

The two Yukawa GMSA approach involves solving Eqs. (1), (6), and (8). Waisman, Hoye, and Stell have worked out the explicit analytical solution in 3D:[30,31]

$$-C(r) = a + br + \frac{1}{2}\eta a r^3 + v_\delta \frac{1-e^{-z_\delta r}}{z_\delta r} + v_\delta^2 \frac{\cosh(z_\delta r)-1}{2rK_\delta z_\delta^2 e^{z_\delta}} + v_\infty \frac{1-e^{-z_\infty r}}{z_\infty r} + v_\infty^2 \frac{\cosh(z_\infty r)-1}{2rK_\infty z_\infty^2 e^{z_\infty}}, \quad r<1, \tag{A1}$$

where a is the dimensionless compressibility defined in Eqs. (3) and (4), the v_i are defined in Eq. (9), and a new

parameter enters:

$$b = \frac{1}{4}\left(-\frac{e^{-z_\delta}v_\delta^2}{K_\delta} - \frac{e^{-z_\infty}v_\infty^2}{K_\infty} - 24\eta g_1^2 + 2v_\delta z_\delta + 2v_\infty z_\infty\right). \tag{A2}$$

We recommend the interested reader consult[30,31] for details of the derivation. To get from Eq. (A1) to Eq. (12) involves taking the appropriate mean field Kac limit, i.e., v_∞ remains finite as $z_\infty \to 0$; the final result requires $K_\infty \to z_\infty^2 v_\infty/(24\eta)$ as $z_\infty \to 0$ based on Eq. (10). Combining Eqs. (A1) and (A2), followed by straightforward manipulations, then yields

$$-C(r) = a + \frac{1}{2}\eta a r^3 + v_\delta\frac{1-e^{-z_\delta r}}{z_\delta r} + v_\delta^2\frac{\cosh(z_\delta r)-1}{2rK_\delta z_\delta^2 e^{z_\delta}}$$

$$+\frac{1}{4}r\left(-\frac{e^{-z_\delta}v_\delta^2}{K_\delta} - 24\eta g_1^2 + 2v_\delta z_\delta\right)$$

$$+ v_\infty + \left[-\frac{re^{-z_\infty}v_\infty^2}{4K_\infty}\right.$$

$$\left.+ v_\infty^2\frac{\cosh(z_\infty r)-1}{2rK_\infty z_\infty^2 e^{z_\infty}}\right]_{\substack{z_\infty\to 0\\ K_\infty\to z_\infty^2 v_\infty/(24\eta)}}, \quad r<1. \tag{A3}$$

The last term in Eq. (A3) is subtle. If one naively sets $z_\infty \to 0$ and did not replace $K_\infty \to z_\infty^2 v_\infty/(24\eta)$, this term would vanish. But, by making the appropriate replacement and Taylor expanding the last term of Eq. (A3) in z_∞, one obtains

$$\left[-\frac{re^{-z_\infty}v_\infty^2}{4K_\infty} + v_\infty^2\frac{\cosh(z_\infty r)-1}{2rK_\infty z_\infty^2 e^{z_\infty}}\right]_{\substack{z_\infty\to 0\\ K_\infty\to z_\infty^2 v_\infty/(24\eta)}}$$

$$= \frac{1}{2}v_\infty\eta r^3 + O(z_\infty). \tag{A4}$$

Combining Eq. (A3) with Eq. (A4) gives the $C(r)$ in Eq. (12).

APPENDIX B: FOURIER TRANSFORMED DIRECT CORRELATION FUNCTION

Equations (11) and (12) allow an analytic expression for $C(k)$ to be derived:

$$C(k) = -4\pi\int_0^1 dr r^2\frac{\sin(kr)}{kr}\left(a + \frac{1}{2}\eta a r^3 + v_\delta\frac{1-e^{-z_\delta r}}{z_\delta r} + v_\delta^2\frac{\cosh(z_\delta r)-1}{2rK_\delta z_\delta^2 e^{z_\delta}}\right)$$

$$-4\pi\int_0^1 dr r^2\frac{\sin(kr)}{kr}\left(\frac{1}{4}r\left(-\frac{v_\delta^2 e^{-z_\delta}}{K_\delta} - 24\eta g_1^2 + 2v_\delta z_\delta\right) + v_\infty + \frac{1}{2}v_\infty\eta r^3\right)$$

$$+4\pi\int_1^\infty dr r^2\frac{\sin(kr)}{kr}K_\delta\frac{e^{-z_\delta(r-1)}}{r} + 4\pi\int_1^\infty dr r^2\frac{\sin(kr)}{kr}\left[K_\infty\frac{e^{-z_\infty(r-1)}}{r}\right]_{\substack{z_\infty\to 0\\ K_\infty\to z_\infty^2 v_\infty/(24\eta)}}. \tag{B1}$$

It is useful to partition Eq. (B1) into two different components: (1) all terms that are nonzero and finite, and (2) the mean field background contribution given by

$$C_\infty(k) \equiv 4\pi\int_1^\infty dr r^2\frac{\sin(kr)}{kr}\left[K_\infty\frac{e^{-z_\infty(r-1)}}{r}\right]_{\substack{z_\infty\to 0\\ K_\infty\to z_\infty^2 v_\infty/(24\eta)}}. \tag{B2}$$

By default, $C_f(k)$ is the total result in Eq. (B1) when subtracting out Eq. (B2), and is given by the complicated form:

$$C_f(k) = \frac{4\pi K_\delta(k\cos(k) + z_\delta\sin(k))}{k^3 + z_\delta^2 k}$$

$$-\frac{1}{kK_\delta z_\delta^2}[\pi e^{-z_\delta}(c_1(k) - c_2(k) + c_3(k) + c_4(k) + c_5(k) + c_6(k) - c_7(k))]$$

$$-\frac{1}{kK_\delta z_\delta^2}[\pi e^{-z_\delta}(-c_8(k) - c_9(k) + c_{10}(k) + c_{11}(k) + c_{12}(k))], \tag{B3}$$

$$c_1(k) = \frac{2v_\delta^2(\cos(k)-1)}{k},$$

$$c_2(k) = \frac{4e^{z_\delta} K_\delta v_\delta z_\delta (\cos(k) - 1)}{k},$$

$$c_3(k) = \frac{4ae^{z_\delta} K_\delta z_\delta^2 (\sin(k) - k\cos(k))}{k^2},$$

$$c_4(k) = \frac{4v_\infty e^{z_\delta} K_\delta z_\delta^2 (\sin(k) - k\cos(k))}{k^2},$$

$$c_5(k) = \frac{v_\delta^2 z_\delta^2 \left(2 + \left(k^2 - 2\right)\cos(k) - 2k\sin(k)\right)}{k^3},$$

$$c_6(k) = \frac{24e^{z_\delta} K_\delta \eta g_1^2 z_\delta^2 \left(2 + \left(k^2 - 2\right)\cos(k) - 2k\sin(k)\right)}{k^3},$$

$$c_7(k) = \frac{2e^{z_\delta} K_\delta v_\delta z_\delta^3 \left(2 + \left(k^2 - 2\right)\cos(k) - 2k\sin(k)\right)}{k^3},$$

$$c_8(k) = \frac{2ae^{z_\delta} K_\delta \eta z_\delta^2 \left(\left(24 - 12k^2 + k^4\right)\cos(k) - 4k\left(k^2 - 6\right)\sin(k) - 24\right)}{k^5},$$

$$c_9(k) = \frac{2v_\infty e^{z_\delta} K_\delta \eta z_\delta^2 \left(\left(24 - 12k^2 + k^4\right)\cos(k) - 4k\left(k^2 - 6\right)\sin(k) - 24\right)}{k^5},$$

$$c_{10}(k) = \frac{e^{-z_\delta} v_\delta^2 (ke^{z_\delta} - k\cos(k) - z_\delta \sin(k))}{k^2 + z_\delta^2},$$

$$c_{11}(k) = \frac{4K_\delta v_\delta z_\delta \left(k\cos(k) + z_\delta \sin(k) - ke^{-z_1}\right)}{k^2 + z_\delta^2},$$

$$c_{12}(k) = \frac{v_\delta^2 (k + e^{z_\delta} (z_\delta \sin(k) - k\cos(k)))}{k^2 + z_\delta^2}.$$

Though cumbersome, the analytic Eq. (B3) renders the analysis much simpler than numerically Fourier transforming Eqs. (11) and (12) which develops a divergence near jamming. Moreover, the k-space DCF is the key quantity in the dynamical vertex of NLE theory.[5–7] Fourier transforming $C_\infty(k)$ or Eq. (B2) requires limits be appropriately taken, leading to

$$C_\infty(k) = \left\{ \begin{array}{ll} \frac{4\pi v_\infty}{24\eta}, & k = 0 \\ 0, & k > 0 \end{array} \right\}. \quad \text{(B4)}$$

The final analytic expression combines Eqs. (B3) and (B4) giving

$$C(k) = C_f(k) + C_\infty(k). \quad \text{(B5)}$$

$C_\infty(k)$ has a *finite* amplitude delta-function-like contribution at $k = 0$. This leads to a subtlety when numerically inverse Fourier transforming to obtain $h(r) = g(r) - 1$. Taking the Fourier transform of Eq. (1) and solving for $h(k)$ gives

$$h(k) = \frac{C(k)}{1 - \rho C(k)}. \quad \text{(B6)}$$

However, numerically what must be evaluated is not $h(k)$, but $h_f(k)$ defined as

$$h_f(k) \equiv \frac{C_f(k)}{1 - \rho C_f(k)}. \quad \text{(B7)}$$

By numerically inverting Eq. (B7), one obtains $h_f(r) \equiv g_f(r) - 1$, and the mean field contribution is missed. Over any finite range though, $g_f(r) = g(r)$, and differences only arise when using Eq. (3) numerically to determine the compressibility. Ultimately, the difference between numerically integrating $h_f(r)$ in Eq. (3) to obtain the compressibility, and what it is enforced to be, must be added in by hand.

APPENDIX C: SELF-CONSISTENT GMSA SOLUTION

Four nonlinear algebraic equations were found by Hoye, Stell, and Waisman relating a, b, v_δ, and v_∞ in Eq. (A1). We refer the reader to Refs. 30 and 31 where these equations were simplified by eliminating some false solutions and linearizing the equations using different variables. Three coupled

algebraic equations result

$$A + \left(1 - \frac{4\gamma_\delta^2}{z_\delta^2}\right) U_0^\delta + \left(1 - \frac{4\gamma_\infty^2}{z_\infty^2}\right) U_0^\infty = q, \tag{C1}$$

$$\left(1 + \frac{4\gamma_\delta^2}{z_\delta^2}\right) A + U_0^\delta + \left(1 + \frac{4(\gamma_\delta - \gamma_\infty)^2}{z_\delta^2 - z_\infty^2}\right) U_0^\infty = \left(\gamma_\delta + \sqrt{q}\right)^2 - \frac{1}{4} z_\delta^2, \tag{C2}$$

$$\left(1 + \frac{4\gamma_\infty^2}{z_\infty^2}\right) A + U_0^\infty + \left(1 - \frac{4(\gamma_\delta - \gamma_\infty)^2}{z_\delta^2 - z_\infty^2}\right) U_0^\delta = \left(\gamma_\infty + \sqrt{q}\right)^2 - \frac{1}{4} z_\infty^2, \tag{C3}$$

where the following new parameters are defined

$$A \equiv (1-\eta)^2 a, \quad q \equiv (1+2\eta)^2/(1-\eta)^2, \quad \gamma_i \equiv 2 - \sqrt{q} - \left(U_1^i/U_0^i\right), \tag{C4}$$

and U_1^i and U_0^i are related to the Yukawa K_i and z_i parameters through

$$K_i = \frac{2(z_i+2)^2 \sigma_i^2}{3\eta z_i^2} U_0^i \left(\frac{U_1^i}{U_0^i} - \alpha_i\right)^2, \tag{C5}$$

where

$$\sigma_i = \frac{1}{2z_i}\left(\frac{z_i - 2}{z_i + 2} + e^{-z_i}\right); \quad \alpha_i = 1 + \frac{z_i^2 \sinh(z_i/2)}{2z_i \cosh(z_i/2) - 4\sinh(z_i/2)}. \tag{C6}$$

Equations (C1)–(C3) specify only the enforcement of the desired compressibility via the parameter A. Two additional equations must be constructed to enforce both the contact value g_1 and the contact derivative Δg_1 relations, which involve the six unknowns in Eqs. (C1)–(C3): U_0^δ, U_0^∞, γ_δ, γ_∞, z_δ, and z_∞. The two new relations constructed by enforcing the desired g_1 and Δg_1[30,31] values are

$$6\eta g_1 = A + U_0^\delta + U_0^\infty - 1, \tag{C7}$$

$$3\eta(\Delta g_1 + g_1) = \frac{(1-4\eta)}{(1-\eta)} A - (\gamma_\delta - 2 + \sqrt{q}) U_0^\delta - (\gamma_\infty - 2 + \sqrt{q}) U_0^\infty - 1. \tag{C8}$$

The final step is to take the $z_\infty \to 0$ limit in Eqs. (C1)–(C3), and in Eqs. (C7) and (C8). A key identity helps to simplify the equations

$$\lim_{z_\infty \to 0} \gamma_\infty = 0. \tag{C9}$$

Using this result in conjunction with taking the $z_\infty \to 0$ limit, Eqs. (C1) and (C3) become identical. Effectively, z_∞ and γ_∞ drop out of the original expressions. Four coupled equations for four unknowns thus enforce the desired conditions as

$$A + \left(1 - \frac{4\gamma_\delta^2}{z_\delta^2}\right) U_0^\delta + U_0^\infty = q, \tag{C10}$$

$$\left(1 + \frac{4\gamma_\delta^2}{z_\delta^2}\right) A + U_0^\delta + \left(1 + \frac{4\gamma_\delta^2}{z_\delta^2}\right) U_0^\infty = (\gamma_\delta + \sqrt{q})^2 - \frac{1}{4} z_\delta^2, \tag{C11}$$

$$6\eta g_1 = A + U_0^\delta + U_0^\infty - 1, \tag{C12}$$

$$3\eta(\Delta g_1 + g_1) = \frac{(1-4\eta)}{(1-\eta)} A - (\gamma_\delta - 2 + \sqrt{q}) U_0^\delta - (-2 + \sqrt{q}) U_0^\infty - 1. \tag{C13}$$

Equations (C12) and (C13) are utilized to obtain U_0^δ and U_0^∞ as explicit functions of γ_δ giving

$$U_0^\delta[\gamma_\delta] = \frac{A(1 + 2\eta + (\eta-1)\sqrt{q}) - (\eta-1)(3\eta\Delta g_1 - 9\eta g_1 + \sqrt{q}(1 + 6\eta g_1) - 1)}{(\eta-1)\gamma_\delta}, \tag{C14}$$

$$U_0^\infty[\gamma_\delta] = \frac{A(\gamma_\delta + \sqrt{q} - \eta(2 + \sqrt{q} + \gamma_\delta) - 1)}{(\eta-1)\gamma_\delta} + \frac{(\eta-1)(3\eta\Delta g_1 + \sqrt{q} + \gamma_\delta - 9\eta g_1 + 6\eta g_1(\sqrt{q} + \gamma_\delta) - 1)}{(\eta-1)\gamma_\delta}, \tag{C15}$$

where square brackets indicate functional dependence on the bracketed variables.

Rearranging Eq. (C10) to solve for z_δ, one finds two solution branches

$$z_\delta[\gamma_\delta] = \pm \frac{2\gamma_\delta \sqrt{U_0^\delta[\gamma_\delta]}}{\sqrt{A - q + U_0^\delta[\gamma_\delta] + U_0^\infty[\gamma_\delta]}}, \tag{C16}$$

where the positive z_δ is the desired solution. All variables except for γ_δ have been eliminated. The only remaining step is to insert Eqs. (C14)–(C16) into Eq. (C11). While not immediately obvious from the complexity of the resulting expression for γ_δ, an analytical solution can be found

$$\gamma_\delta = \frac{-(\gamma_1 - \gamma_2 \cdot \gamma_3 + \gamma_4(\gamma_5 + \gamma_6 - \gamma_7 + \gamma_8 + \gamma_9))}{(\gamma_{10}(\gamma_{11} + \gamma_{12}))}, \tag{C17}$$

$$\gamma_1 = A^2\left(1+2\eta+(\eta-1)\sqrt{q}\right)^2,$$
$$\gamma_2 = 2A(\eta-1)\left(1+2\eta+(\eta-1)\sqrt{q}\right),$$
$$\gamma_3 = 3\Delta g_1\eta - 9\eta g_1 + \sqrt{q}(2-q+12\eta g_1) - 1,$$
$$\gamma_4 = (\eta-1)^2,$$
$$\gamma_5 = 2+9\Delta g_1^2\eta^2 - q^2(1+6\eta g_1),$$
$$\gamma_6 = q(1+6\eta g_1)^2 + 2q^{3/2}(1+9\eta g_1),$$
$$\gamma_7 = 4\sqrt{q}(1+6\eta g_1)(1+9\eta g_1),$$
$$\gamma_8 = 9\eta g_1(4+3\eta g_1(7+8\eta g_1)),$$
$$\gamma_9 = 6\Delta g_1\eta\left(\sqrt{q}(2-q+12\eta g_1) - 9\eta g_1 - 1\right),$$
$$\gamma_{10} = (\eta-1)(1-q+6\eta g_1),$$
$$\gamma_{11} = A\left(\sqrt{q}-\eta\left(2+\sqrt{q}\right)-1\right),$$
$$\gamma_{12} = (\eta-1)\left(3\Delta g_1\eta - 9\eta g_1 + \sqrt{q}(1+6\eta g_1) - 1\right).$$

Equations (C14)–(C17) determine the four unknown parameters U_0^δ, U_0^∞, γ_δ, and z_δ, at a given η, for the desired parameters a, g_1, and Δg_1. With the four unknowns, Eqs. (C4)–(C6) provide K_δ, but not K_∞ since it is infinitesimal based on the mean field treatment of the long range direct correlation function tail. Instead, the relevant parameter for the latter is v_∞ (see Sec. II B) which is nonzero and finite and can be computed from Eqs. (C4)–(C6) by directly evaluating v_∞ and taking the $z_\infty \to 0$ limit. We find

$$v_\infty = \frac{\left(U_1^\infty - 4U_0^\infty\right)^2}{9U_0^\infty}, \tag{C18}$$

$$U_1^\infty = (2-\sqrt{q})U_0^\infty. \tag{C19}$$

This completes the derivation of the fully analytic solution to the two Yukawa mean field self-consistent GMSA closure theory.

APPENDIX D: JAMMED HARD SPHERE RDF CONTACT DERIVATIVE

Recall the concept of cavity particles as objects that behave as if they are hard spheres when interacting with the surrounding fluid, but have no interaction with one another and hence can overlap. In the following derivation of the contact derivative of $g(r)$, a pair of cavity particles is dissolved at infinite dilution in the hard sphere fluid as illustrated in Figure 12. Although our focus is 3-dimensions, we find it is possible to analyze this problem in arbitrary dimension. Since the latter may be of use for future possible extension of the full GMSA and NLE theories beyond 3D, we present a general derivation.

For economy of expression in this appendix, lengths and densities are treated as dimensionless since the unit length $\sigma = 1$. If the two cavities overlap perfectly the stress, S_D, (divided by k_BT/σ^D) at the surface χ is[53]

$$S_D = \rho g(1), \tag{D1}$$

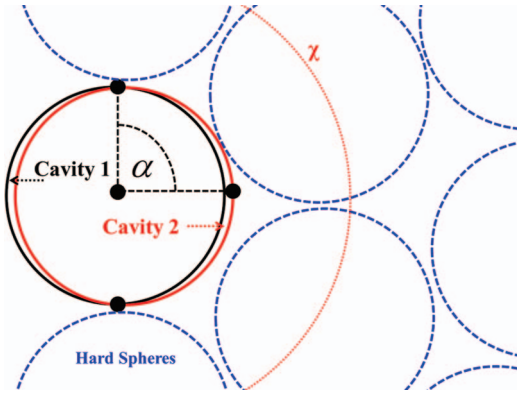

FIG. 12. 2D representation of 3D cavity particles 1 and 2 an infinitesimal distance apart (small separation shown for clarity). Cavity particle 2 experiences a thermodynamic force pushing it into particle 1 from collisions with hard sphere particles at the available surface χ (only half of the surface since the other half lies infinitesimally within cavity 1).

which follows from the general expression for the pure kinetic (momentum transfer) stress felt by a D dimensional sphere

$$S_D = -\int_1^\infty r^{D-1}\rho g(r)\left(\frac{du_{HS}(r)}{dr}\right)dr, \tag{D2}$$

where $u_{HS}(r)$ is the hard sphere potential divided by k_BT. Near jamming Eq. (D2) can be expressed in another form since

$$\lim_{\eta\to\eta_j} g(r) = \frac{Z_c\delta(r-1)}{\rho_j s_D(1)}, \quad r\sim 1, \tag{D3}$$

where $s_D(1) = 2\pi^{D/2}/\Gamma(D/2)$ is the surface area of a D dimensional sphere of unit radius, $\Gamma(x)$ is the Gamma function, and ρ_j the jamming density. Using Eq. (D3) in Eq. (D2) we find

$$S_D = -Z_c\frac{\Gamma(D/2)}{2\pi^{D/2}}\left(\frac{du_{HS}(r)}{dr}\right)_{r=1}. \tag{D4}$$

Of course, $(du_{HS}(r)/dr)_{r=1}$ is formally ill-defined, but some exact statements can be made regarding it in a limiting sense. At jamming, the hard sphere contact potential of mean force (divided by k_BT/σ), defined as[53]

$$F(1) = \left.\frac{d\ln g(r)}{dr}\right|_{r=1} \tag{D5}$$

is related to the force between two contacting hard spheres and *must* satisfy force balancing yielding

$$F(1) = \left.\frac{d\ln g(r)}{dr}\right|_{r=1} = \left.\frac{du_{HS}(r)}{dr}\right|_{r=1}, \tag{D6}$$

which is a strictly *necessary* equality.

Further progress requires the functional dependence of $d\ln g(r)/dr|_{r=1}$ on $g(1)$. To approximately extract this we construct a linear lower bound (LB) $g_{LB}(r)$ on the radial

distribution delta function satisfying $g_\delta(r) \geq g_{LB}(r)$ as

$$g_{LB}(r) \equiv \begin{cases} g(1) + G(r-1), & 1 \leq r \leq 1 - g(1)/G \\ 0, & r > 1 - g(1)/G, \end{cases} \quad \text{(D7)}$$

where $G \equiv dg(r)/dr|_{r=1}$. Now, $g_\delta(r)$ must be finite integrable in a D dimensional space, which suggests the LB must also be, thereby requiring

$$\int_1^{1-g(1)/G} dr r^{D-1} g_{LB}(r) \neq 0 \quad \text{or} \quad \infty. \quad \text{(D8)}$$

Near or at jamming $g_{LB}(r)$ is rapidly varying compared to r^{D-1} allowing the replacement of r^{D-1} in Eq. (D8) with unity and integration yields

$$\int_1^{1-g(1)/G} dr g_{LB}(r) = -\frac{g^2(1)}{2G}, \quad \text{(D9)}$$

which suggests $G \equiv dg(r)/dr|_{r=1} \propto g^2(1)$ for finite integrable behavior for *all* D.

Using Eq. (D6) in Eq. (D4) and postulating that

$$\left.\frac{d \ln g(r)}{dr}\right|_{r=1} = -Qg(1), \quad \text{(D10)}$$

where Q is a constant, we find by equating to Eq. (D1)

$$S_D = Z_c \frac{\Gamma(D/2)}{2\pi^{D/2}} Qg(1) = \eta_j \frac{\Gamma(1+D/2)}{\pi^{D/2}(1/2)^D} g(1), \quad \text{(D11)}$$

where $\rho = \eta\Gamma(1+D/2)\pi^{-D/2}(1/2)^{-D}$ was used. Equation (D11) is easily solved for the unknown constant Q giving at jamming

$$\left.\frac{d \ln g(r)}{dr}\right|_{r=1} = -\frac{D2^D\eta_j}{Z_c} g(1). \quad \text{(D12)}$$

Note that for an isostatic packing $Z_c = Z_{c,iso} \equiv 2D$, and we thus find

$$\left.\frac{d \ln g(r)}{dr}\right|_{r=1} = -2^{D-1}\eta_j g(1), \quad Z_c = Z_{c,iso}. \quad \text{(D13)}$$

Supporting evidence that Eq. (D12) is exact can be seen in Figure 13 for $D = 3$ where $Z_c(r)$ is plotted using $Z_c = 4$, 6, 8, and 10 in Eq. (D12) giving $F(0) = -6\eta g_1$, $-4\eta g_1$, $-3\eta g_1$, and $-2.4\eta g_1$, respectively. These four contact derivatives are enforced in the GMSA closure to generate the four $Z_c(r)$ curves in Figure 13 using the equilibrium densest glass of Ref. 1. Clearly, the GMSA approach gives step-like functions that approach 4, 6, 8, and 10 as expected. This result, though seemingly obvious, is non-trivial as Eq. (D12) was derived without knowledge of the GMSA closure. Apparently, the equilibrium-based GMSA closure contains information about how the near contact region behaves near jamming. We believe that Eq. (D12) is exact in equilibrium and can be derived in two separate ways while agreeing with our approximate, though seemingly accurate, equilibrium GMSA hard sphere integral equation theory.

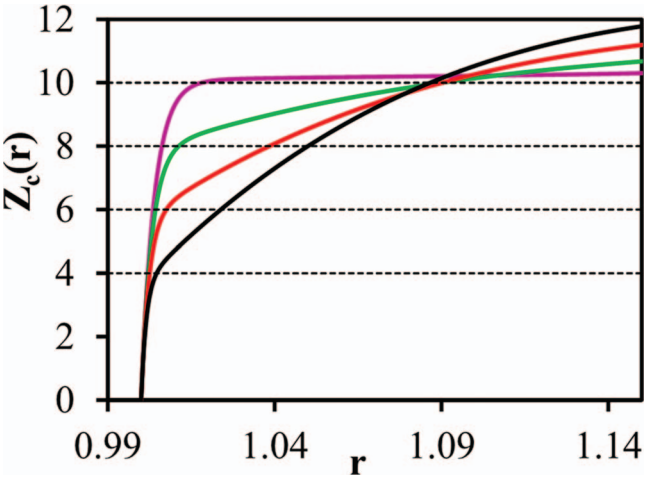

FIG. 13. Demonstration that Eqs. (17) and (D12) are correct within the GMSA approach. In order from bottom to top (left side) the corresponding contact derivatives are $F(0) = -6\eta g_1$, $-4\eta g_1$, $-3\eta g_1$, and $-2.4\eta g_1$ giving the expected values $Z_c = 4$, 6, 8, and 10. The volume fraction was fixed for all cases corresponding to $\eta = 0.663$ while using the contact value and compressibility from the equilibrium glass developed in Ref. 1.

[1]R. Jadrich and K. S. Schweizer, J. Chem. Phys. **139**, 054501 (2013).
[2]G. Parisi and F. Zamponi, Rev. Mod. Phys. **82**, 789 (2010); M. Mezard and G. Parisi, J. Chem. Phys. **111**, 1076 (1999); H. Yoshino, *ibid.* **136**, 214108 (2012).
[3]H. Jacquin, L. Berthier, and F. Zamponi, Phys. Rev. Lett. **106**, 135702 (2011); Phys. Rev. E **84**, 051103 (2011).
[4]W. Götze and L. Sjogren, Rep. Prog. Phys. **55**, 241 (1992); W. Gotze, *Complex Dynamics of Glass Forming Liquids: A Mode Coupling Theory Approach* (Oxford University Press, Oxford, 2008).
[5]K. S. Schweizer, J. Chem. Phys. **123**, 244501 (2005); K. S. Schweizer and E. J. Saltzman, *ibid.* **119**, 1181 (2003).
[6]K. S. Schweizer, Curr. Opin. Colloid Interface Sci. **12**, 297 (2007); E. J. Saltzman and K. S. Schweizer, Phys. Rev. E **77**, 051504 (2008).
[7]K. S. Schweizer and G. Yatsenko, J. Chem. Phys. **127**, 164505 (2007).
[8]For recent reviews see S. Torquato and F. H. Stillinger, Rev. Mod. Phys. **82**, 2633 (2010); A. J. Liu and S. R. Nagel, Ann. Rev. Condens. Matter Phys. **1**, 347 (2010).
[9]A. Donev, F. H. Stillinger, and S. Torquato, Phys. Rev. Lett. **95**, 090604 (2005).
[10]A. B. Hopkins, F. H. Stillinger, and S. Torquato, Phys. Rev. E **86**, 021505 (2012); É. Marcotte, F. H. Stillinger, and S. Torquato, J. Chem. Phys. **138**, 12A508 (2013).
[11]C. S. O'Hern, L. E. Silbert, A. J. Liu, and S. R. Nagel, Phys. Rev. E **68**, 011306 (2003).
[12]A. Donev, S. Torquato, and F. H. Stillinger, Phys. Rev. E **71**, 011105 (2005).
[13]M. D. Rintoul and S. Torquato, J. Chem. Phys. **105**, 9258 (1996).
[14]J. P. Hansen and I. R. McDonald, *Theory of Simple Liquids*, 2nd ed. (Academic Press, London, 1986).
[15]D. A. McQuarrie, *Statistical Mechanics* (University Science Books, Sausalito, CA, 2000).
[16]For recent reviews see A. Cavagna, Phys. Rep. **476**, 51 (2009); L. Berthier and G. Biroli, Rev. Mod. Phys. **83**, 587 (2011); V. Lubchenko and P. G. Wolynes, Ann. Rev. Phys. Chem. **58**, 235 (2007).
[17]See, for example, G. S. Cargill, J. Appl. Phys. **41**, 2248 (1970); H. R. Wendt and F. F. Abraham, Phys. Rev. Lett. **41**, 1244 (1978); Y. Hitawari, J. Phys. C **13**, 5899 (1980).
[18]G. Brambilla, D. El Masri, M. Pierno, L. Berthier, L. Cipelletti, G. Petekidis, and A. B. Schofield, Phys. Rev. Lett. **102**, 085703 (2009).
[19]P. N. Pusey and W. van Megen, Phys. Rev. Lett. **59**, 2083 (1987); W. van Megen, T. C. Mortensen, S. R. Williams, and J. Müller, Phys. Rev. E **58**, 6073 (1998).

[20]G. Odriozola and L. Berthier, J. Chem. Phys. **134**, 054504 (2011).
[21]L. Berthier and T. A. Witten, Phys. Rev. E **80**, 021502 (2009).
[22]M. Hermes and M. Dijkstra, Europhys. Lett. **89**, 38005 (2010).
[23]M. Skoge, A. Donev, F. H. Stillinger, and S. Torquato, Phys. Rev. E **74**, 041127 (2006).
[24]G. Pérez-Ángel, L. E. Sánchez-Díaz, P. E. Ramírez-González, R. Juárez-Maldonado, A. Vizcarra-Rendón, and M. Medina-Noyola, Phys. Rev. E **83**, 060501(R) (2011).
[25]P. Tarazona, Mol. Phys. **52**, 871 (1984).
[26]Y. Singh, J. P. Stoessel, and P. G. Wolynes, Phys. Rev. Lett. **54**, 1059 (1985).
[27]D. Henderson and E. W. Grundke, J. Chem. Phys. **63**, 601 (1975).
[28]M. Dennison, A. J. Masters, D. L. Cheung, and M. P. Allen, Mol. Phys. **107**, 375 (2009).
[29]E. Waisman, Mol. Phys. **25**, 45 (1973).
[30]J. S. Høye and G. Stell, Mol. Phys. **32**, 195 (1976).
[31]J. S. Høye, G. Stell, and E. Waisman, Mol. Phys. **32**, 209 (1976); J. S. Høye and G. Stell, *ibid*. **52**, 1057 (1984).
[32]D. M. Heyes, M. Cass, A. C. Brańka, and H. Okumura, J. Phys.: Condens. Matter **18**, 7553 (2006).
[33]J. Kolafa, S. Labik, and A. l. Malijevsky, Phys. Chem. Chem. Phys. **6**, 2335 (2004); D. Ayala de Lonngi and P. A. L. Villanueva, Mol. Phys. **73**, 763 (1991).
[34]N. F. Carnahan and K. E. Starling, J. Chem. Phys. **51**, 635 (1969).
[35]Y. Song, E. A. Mason, and R. M. Stratt, J. Phys. Chem. **93**, 6916 (1989).
[36]M. Bishop and P. A. Whitlock, J. Chem. Phys. **123**, 014507 (2005); J. Stat. Phys. **126**, 299 (2007); M. Bishop, N. Clisby, and P. A. Whitlock, J. Chem. Phys. **128**, 034506 (2008).
[37]M. Heying and D. S. Corti, J. Phys. Chem. B **108**, 19756 (2004).
[38]H. Reiss, H. L. Frisch, and J. L. Lebowitz, J. Chem. Phys. **31**, 369 (1959).
[39]T. R. Kirkpatrick and P. G. Wolynes, Phys. Rev. A **35**, 3072 (1987).
[40]R. Zwanzig, *Nonequilibrium Statistical Mechanics* (Oxford University Press, Oxford, 2001).
[41]R. Sear, J. Chem. Phys. **113**, 4732 (2000).
[42]V. Kobelev and K. S. Schweizer, Phys. Rev. E **71**, 021401 (2005).
[43]R. Rao, V. Kobelev, Q. Li, J. A. Lewis, and K. S. Schweizer, Langmuir **22**, 2441 (2006).
[44]G. Nägele and J. Bergenholtz, J. Chem. Phys. **108**, 9893 (1998).
[45]P. Charbonneau, A. Ikeda, G. Parisi, and F. Zamponi, Phys. Rev. Lett. **107**, 185702 (2011); P. Charbonneau, E. I. Corwin, G. Parisi, and F. Zamponi, *ibid*. **109**, 205501 (2012); P. Charbonneau, A. Ikeda, G. Parisi, and F. Zamponi, Proc. Natl. Acad. Sci. U.S.A. **109**, 13939 (2012).
[46]M. Wyart, Phys. Rev. Lett. **109**, 125502 (2012).
[47]R. D. Grooer, J. P. van der Eerden, and N. M. Faber, J. Chem. Phys. **87**, 2263 (1987).
[48]L. Berthier and G. Tarjus, Eur. Phys. J. E **34**, 96 (2011).
[49]S. Mirigian and K. S. Schweizer, "Microscopic theory of activated relaxation in liquids over 14 decades in time" (unpublished).
[50]P. Rabochiy and V. Lubchenko, J. Chem. Phys. **138**, 12A534 (2013).
[51]R. C. Kramb, R. Zhang, K. S. Schweizer, and C. F. Zukoski, Phys. Rev. Lett. **105**, 055702 (2010).
[52]H. C. Andersen, J. D. Weeks, and D. Chandler, Phys. Rev. A **4**, 1597 (1971).
[53]E. Meeron and A. J. F. Siegert, J. Chem. Phys. **48**, 3139 (1968).